Optical conductivity of a Dirac-Fermi liquid

Prachi Sharma [1], Alessandro Principi [2] and Dmitrii L. Maslov [1]
[1] Department of Physics, University of Florida, Gainesville, Florida 32611-8440, USA
[2] Department of Physics and Astronomy, University of Manchester, Oxford Road, M13 9PL Manchester, United Kingdom

(Received 19 January 2021; revised 29 May 2021; accepted 6 July 2021; published 26 July 2021)

A Dirac-Fermi liquid (DFL), a doped system with Dirac spectrum, is an important example of a non-Galilean-invariant Fermi liquid (FL). Real-life realizations of a DFL include, e.g., doped graphene, surface states of three-dimensional (3D) topological insulators, and 3D Dirac/Weyl metals. We study the optical conductivity of a DFL arising from intraband electron-electron scattering. It is shown that the effective current relaxation rate behaves as $1/\tau_J \propto (\omega^2 + 4\pi^2T^2)(3\omega^2 + 8\pi^2T^2)$ for $\max\{\omega, T\} \ll \mu$, where μ is the chemical potential, with an additional logarithmic factor in two dimensions. In graphene, the quartic form of $1/\tau_J$ competes with a small FL-like term, $\propto \omega^2 + 4\pi^2T^2$, due to trigonal warping of the Fermi surface. We also calculated the dynamical charge susceptibility $\chi_c(\mathbf{q}, \omega)$ outside the particle-hole continua and to one-loop order in the dynamically screened Coulomb interaction. For a two-dimensional DFL, the imaginary part of $\chi_c(\mathbf{q}, \omega)$ scales as $q^2\omega \ln |\omega|$ and q^4/ω^3 for frequencies larger and smaller than the plasmon frequency at given q, respectively. The small-q limit of $\mathrm{Im}\,\chi_c(\mathbf{q}, \omega)$ reproduces our result for the conductivity via the Einstein relation.

DOI: 10.1103/PhysRevB.104.045142

I. INTRODUCTION

The optical conductivity of a Fermi liquid (FL) is described by the Gurzhi form [1]

$$\mathrm{Re}\sigma(\omega, T) = \sigma_G\left(1 + \frac{4\pi^2T^2}{\omega^2}\right). \tag{1}$$

(In what follows, we set $k_B = 1$ and $\hbar = 1$.) Despite its generality, Eq. (1) does not apply to all types of FLs. For example, it obviously does not apply to a Galilean-invariant FL, i.e., a single-band system with a parabolic dispersion. In the latter case, momentum conservation automatically implies current conservation, and thus $\mathrm{Re}\sigma(\omega, T) = 0$. The minimal condition for Eq. (1) to apply is a sufficiently strong violation of Galilean invariance. If umklapp scattering is allowed, Eq. (1) applies automatically. However, it can also apply even if umklapp scattering is forbidden. Namely, it applies to a three-dimensional (3D) FL with a Fermi surface (FS) that deviates from an ellipsoidal shape [2,3] to a two-dimensional (2D) FL with a concave FS [2,4–11] and to a multiply connected FS, both in 2D and 3D [3]. Universality of Eq. (1) is protected by the first Matsubara-frequency rule [12], which stipulates that $\mathrm{Re}\sigma(\pm 2i\pi T, T) = 0$. We will refer to a FL with optical conductivity described by Eq. (1) as to a "conventional" one.

If the conditions specified above are not satisfied, a FL belongs to an intermediate class, which we will dub as a "partially Galilean-invariant FL." Examples include a FL with isotropic but nonparabolic dispersion (both in 2D and 3D), and a 2D FL with a singly connected and convex FS. A prominent member of this class is a Dirac-Fermi liquid (DFL), i.e., a system with isotropic and linear dispersion doped away from the Dirac point, which is the focus of this paper. Examples of a DFL are provided by gated monolayer graphene [13], surface states of 3D topological insulators [14], and doped Dirac and Weyl metals in 3D [15–17]. The single-particle and thermodynamic properties of conventional and partially Galilean-invariant FLs are very much alike; the same is true for viscosity and thermal conductivity. However, their electrical conductivity is very much different. A linear dispersion in a DFL implies that Galilean invariance is broken and thus dissipation at finite frequency is possible. However, dissipation in a DFL is weaker than in a conventional FL because the interaction between electrons right on the FS does not relax the current.

In this paper, we show that the dissipative part of the optical conductivity of a DFL is described by the scaling form

$$\mathrm{Re}\sigma(\omega, T) = \sigma_D\frac{\omega^2}{\mu^2}\left(1 + \frac{4\pi^2T^2}{\omega^2}\right)\left(3 + \frac{8\pi^2T^2}{\omega^2}\right)S(\omega, T), \tag{2}$$

where μ is the chemical potential (assumed to be the largest energy scale in the problem), and $S(\omega, T)$ varies with ω and T logarithmically in 2D, and is constant in 3D. Note that $\mathrm{Re}\sigma(\pm 2\pi iT, T) = 0$, in agreement with the first Matsubara-frequency rule [12]. The difference between the Gurzhi form in Eq. (1) and the DFL form in Eq. (2) is especially prominent at $T = 0$. In this case, the conductivity of a conventional FL does not depend on ω, while the conductivity of a DFL is small in proportion to $(\omega/\mu)^2 \ll 1$. In fact, Eq. (2) is valid for any partially Galilean-invariant FL; particular details affect only coefficient σ_D and $S(\omega, T)$. For an isotropic FL, σ_D is proportional to (the square of) the "nonparabolicity coefficient," defined as

$$w = 1 - \frac{m^*}{\bar{m}}, \tag{3}$$

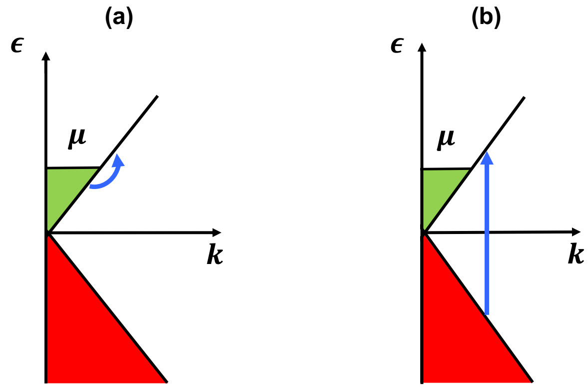

FIG. 1. Intraband (a) and interband (b) optical transitions in a Dirac metal.

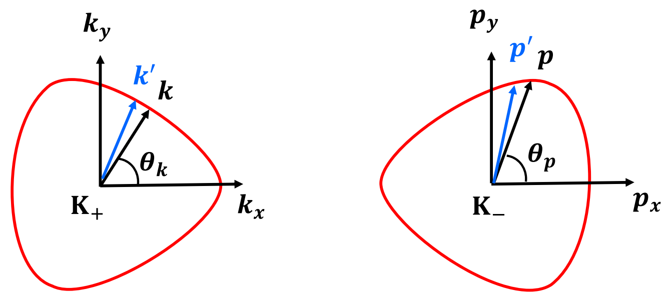

FIG. 2. An intervalley scattering process. The two Fermi surfaces (red) with trigonal warping are located at two adjacent K_+ and K_- points in the Brillouin zone of graphene. **k** and **k**′ are the initial and final momenta of an electron in the K_+ valley. Similarly, **p** and **p**′ are the initial and final momenta in the K_- valley.

where $m^* = k_F/\epsilon'(k_F)$, $1/\bar{m} = \epsilon''(k_F)$, $\epsilon(k)$ is the electron dispersion, and k_F is the Fermi momentum. For a Galilean-invariant system, the dispersion is parabolic, hence $m^* = \bar{m}$, and there is no dissipation even at finite ω. For any other dispersion, $w \neq 0$; in particular, $w = 1$ for the Dirac dispersion.

Phenomenologically, the optical conductivity can be described by the current relaxation time $\tau_J(\omega, T)$, defined by

$$\mathrm{Re}\sigma(\omega, T) \propto \frac{1}{\omega^2 \tau_J(\omega, T)}. \tag{4}$$

With this definition

$$\frac{1}{\tau_J(\omega, T)} \propto \omega^2 + 4\pi^2 T^2 \tag{5}$$

for a conventional FL, while

$$\frac{1}{\tau_J(\omega, T)} \propto (\omega^2 + 4\pi^2 T^2)(3\omega^2 + 8\pi^2 T^2) S(\omega, T) \tag{6}$$

for a DFL. The quartic (as opposed to quadratic) scaling of $1/\tau_J$ was noted in a number of studies, mostly of 2D systems [2–8,11]. It arises because the quadratic term in $1/\tau_J$ vanishes once electrons are projected onto the FS, and one has to go further away from the FS to obtain a finite result.

To be specific, in this paper we focus on doped monolayer graphene. Optical response of graphene has been a subject of extensive research; see, e.g., reviews in Refs. [18–21]. At the level of noninteracting electrons, the optical conductivity of graphene is given by a universal form [22–25]

$$\mathrm{Re}\sigma(\omega) = \frac{e^2}{4}\theta(|\omega| - 2\mu), \tag{7}$$

where we assume that $\mu \geqslant 0$ without the loss of generality. The absorption threshold at $\omega = 2\mu$ is due to Pauli blocking of states available for transitions between the lower and upper Dirac cones (cf. Fig. 1). The optical conductivity of graphene in the near-infrared and optical ranges, i.e, far above the Pauli threshold of 2μ, is indeed observed to be close to the universal value of $e^2/4$ [26–29]. However, experimentally one also observes significant absorption at $\omega \lesssim 2\mu$ [21,27,28,30], which would be absent in ideal graphene. Certainly, some of this absorption is due to extrinsic scattering mechanisms, e.g., impurity scattering. However, there is still significant absorption even at frequencies exceeding the width of the Drude peak. That, and also the fact that at higher frequencies the conductivity scales with ω/μ [18], prompts one to think about intrinsic mechanisms as well.

On the theoretical side, a large number of authors studied the deviation of the conductivity of graphene at the Dirac point from the universal value due to electron-electron (*ee*) interaction [18,20,31–38]. Absorption below the Pauli threshold in doped systems has also been addressed theoretically, but in fewer studies. In Refs. [39–42], it was shown that about 50% of absorption can be explained by scattering of electrons (or holes) by disorder, with an additional contribution of excitonic effects [42]. Many-body effects in intraband absorption were considered in Refs. [37,43,44]. The most relevant to our study is the one by Principi *et al.* [44], whose result for the $T = 0$ optical conductivity of graphene agrees with ours, up to a factor of $\ln \omega$ and the dependence on the coupling constant.

The rest of our paper is organized as follows. Our model is outlined in Sec. II. In lieu of calculating the diagrams generated by the Kubo formula, we adopt a method that allows one to calculate the dissipative part of the conductivity by using the exact Heisenberg equations of motion [7,8,45]. This method is described in Sec. III A. In Sec. III B, we show that if the 2D Fermi surfaces around each of the Dirac points are approximated by circles, the optical conductivity is of the form given in Eq. (2) with

$$\sigma_D = \frac{e^2}{240\pi^2} \text{ and } S(\omega, T) = \ln \frac{v_D \kappa}{\max\{|\omega|, T\}}, \tag{8}$$

where v_D is the group velocity of Dirac fermions and κ is the (inverse) screening radius. To reiterate, Eqs. (2) and (8) are valid only in the FL regime, i.e., for $\max\{\omega, T\} \ll v_D\kappa \lesssim \mu$. However, they allow one to obtain an order-of-magnitude estimate for the conductivity at the Dirac point by putting $\omega \sim T \sim \mu$. This yields $\sigma \sim e^2$, consistent with prior results for the conductivity of an interacting system of Dirac fermions at the Dirac point [34,35,46].

We also considered the effect of trigonal warping (Sec. III C), which restores the conventional FL behavior. A trigonally warped FS is still convex (cf. Fig. 2), and thus intravalley scattering contributes only the $\max\{\omega^4, T^4\}$ term to $1/\tau_J$ [2]. However, the valleys are not degenerate, and intervalley scattering does give rise to a conventional FL term $1/\tau_J \propto \max\{\omega^2, T^2\}$. The corresponding contribution to the optical conductivity is of the Gurzhi form [Eq. (1)] but with a small prefactor of $(k_F a)^2$, where a is the lattice spacing.

In Sec. IV, we analyze an interplay between *ee* and electron-impurity (*ei*) scattering channels at the level of the Boltzmann equation. We show that if *ee* scattering is the dominant mechanism, the optical conductivity is described by the sum of two Drude peaks, with widths given by the *ee* and *ei* scattering rates, i.e., the *ee* and *ei* channels act as two resistors connected in parallel. If *ei* scattering dominates, the optical conductivity is described by a single Drude peak with a width given by the sum of the *ee* and *ei* scattering rates, i.e., the *ee* and *ei* channels act as two resistors connected in series. As a limiting case, we also derive the T dependence of the dc resistivity. The resistivity increases as $T^4 \ln T$ above the residual value at the lowest T, reaches a maximum at some T that corresponds to comparable *ee* and *ei* scattering rates, and finally goes down back exactly to the residual value at higher T. In Sec. V, we calculate the dynamical charge susceptibility of a DFL, $\chi_c(\mathbf{q},\omega)$. We show that $\mathrm{Im}\,\chi_c(\mathbf{q},\omega)$ scales as $q^2\omega \ln|\omega|$ for $\omega \gg \omega_p(q)$, where $\omega_p(q)$ is the plasmon frequency at given q, and as q^4/ω^3 for $\omega \ll \omega_p(q)$. Via the the Einstein relation, the $q^2\omega \ln|\omega|$ scaling of the charge susceptibility implies that at $q = 0$ the conductivity of a DFL scales as $\omega^2 \ln|\omega|$, in agreement with the result of a direct calculation. Other Dirac systems, bilayer graphene, the surface state of a 3D topological insulator, and 3D Weyl/Dirac semimetals, as well as a relation of our results to the experiment are discussed in Sec. VI. Our conclusions are presented in Sec. VII.

II. DOPED MONOLAYER GRAPHENE

One of the most popular examples of DFL is a doped monolayer graphene (MLG). We begin with the noninteracting tight-binding Hamiltonian [13]

$$H_0 = -\gamma_0 \sum_{s,\langle i,j\rangle} [a_s^\dagger(\mathbf{R}_i) b_s(\mathbf{R}_j) + \text{H.c.}] - \mu \sum_i \hat{n}(\mathbf{R}_i), \quad (9)$$

where $a_s(\mathbf{R}_i)$ and $b_s(\mathbf{R}_i)$ are the fermionic operators corresponding to A and B sublattices, $\langle i, j\rangle$ imply summation over the nearest neighbors, s labels spin, μ is the chemical potential, γ_0 is the coupling constant for hopping between A and B sites, and $\hat{n}(\mathbf{R}_i) = \sum_s a_s^\dagger(\mathbf{R}_i)a_s(\mathbf{R}_i) + b_s^\dagger(\mathbf{R}_i)b_s(\mathbf{R}_i)$ is the number-density operator. In the momentum space, the Hamiltonian is given by

$$H_0 = -\gamma_0 \sum_{s,\mathbf{k}} \Phi_\mathbf{k} a_{\mathbf{k},s}^\dagger b_{\mathbf{k},s} + \text{H.c.} - \mu(a_{\mathbf{k},s}^\dagger a_{\mathbf{k},s} + b_{\mathbf{k},s}^\dagger b_{\mathbf{k},s}), \quad (10)$$

where

$$\Phi_\mathbf{k} = \sum_{i=1}^3 e^{i\mathbf{k}\cdot\delta_i} = e^{ik_y a} + 2e^{-i\frac{k_y a}{2}} \cos\left(\frac{\sqrt{3}}{2}k_x a\right) \quad (11)$$

is a form factor obtained by summation over the nearest neighbors, connected by vectors $\delta_1 = (0, a)$, $\delta_2 = (-\sqrt{3}a/2, -a/2)$, and $\delta_3 = (\sqrt{3}a/2, -a/2)$, and a is the carbon-carbon distance. The Hamiltonian is diagonalized by introducing a new basis [47]

$$a_{\mathbf{k},s} = \frac{e^{i\phi_\mathbf{k}}}{\sqrt{2}}(\alpha_{\mathbf{k},s} + \beta_{\mathbf{k},s}),$$
$$b_{\mathbf{k},s} = \frac{1}{\sqrt{2}}(\beta_{\mathbf{k},s} - \alpha_{\mathbf{k},s}), \quad (12)$$

where $\alpha_{\mathbf{k},s}$ ($\beta_{\mathbf{k},s}$) denotes the annihilation operator of electron (hole) in the conduction (valence) band, and $\phi_\mathbf{k}$ is defined by $\Phi_\mathbf{k} = |\Phi_\mathbf{k}|e^{i\phi_\mathbf{k}}$. In the new basis, the Hamiltonian is just the sum of the conduction and valence band parts:

$$H_0 = \sum_{\mathbf{k}s} (\epsilon_\mathbf{k} - \mu)\alpha_{\mathbf{k},s}^\dagger \alpha_{\mathbf{k},s} + (-\epsilon_\mathbf{k} - \mu)\beta_{\mathbf{k},s}^\dagger \beta_{\mathbf{k},s}, \quad (13)$$

where $\epsilon_\mathbf{k} = \gamma_0|\Phi_\mathbf{k}|$.

We will be interested in low-energy Dirac fermions with momenta near two inequivalent Dirac points $\mathbf{K}_{\varsigma=\pm} = (\varsigma 4\pi/(3\sqrt{3}a), 0)$. Near these points, $\Phi_\mathbf{k}$ can be expanded as

$$\Phi_{\mathrm{K}_\varsigma+\mathbf{p}} \equiv \Phi_{\varsigma,\mathbf{p}} = -\frac{3a}{2}(\varsigma p_x - ip_y) + \frac{3a^2}{8}(\varsigma p_x + ip_y)^2. \quad (14)$$

The last $O(a^2)$ term describes trigonal warping. The low-energy 4×4 Hamiltonian can be written as the sum of the Dirac and trigonal-warping (TW) parts

$$H_0 = H_\mathrm{D} + H_\mathrm{TW}, \quad (15a)$$
$$H_\mathrm{D} = \sum_{\mathbf{p},s} \Psi_{\mathbf{p},s}^\dagger [v_\mathrm{D}\mathbf{p}\cdot(\tau_z \otimes \boldsymbol{\sigma}) - \mu(\tau_0 \otimes \sigma_0)]\Psi_{\mathbf{p},s}, \quad (15b)$$
$$H_\mathrm{TW} = -\frac{v_\mathrm{D}a}{4} \sum_{\mathbf{p},s} \Psi_{\mathbf{p},s}^\dagger \big[\big(p_x^2 - p_y^2\big)(\tau_0 \otimes \sigma_x) - 2p_x p_y(\tau_0 \otimes \sigma_y)\big]\Psi_{\mathbf{p},s}, \quad (15c)$$

where $v_\mathrm{D} = 3\gamma_0 a/2$ is the Dirac velocity, $\boldsymbol{\tau}$ and $\boldsymbol{\sigma}$ are the Pauli matrices which operate in the valley and sublattice spaces, respectively, τ_0 and σ_0 are the identity matrices, and

$$\Psi_{\mathbf{p},s}^\dagger = (\psi_{\mathbf{K}_++\mathbf{p},s}^\dagger, \psi_{\mathbf{K}_-+\mathbf{p},s}^\dagger) = (a_{+,\mathbf{p},s}^\dagger, b_{+,\mathbf{p},s}^\dagger, b_{-,\mathbf{p},s}^\dagger, a_{-,\mathbf{p},s}^\dagger) \quad (16)$$

is a 4-spinor describing the states near the $K_\pm$ point. With trigonal warping taken into account, the energy spectrum is given by

$$\epsilon_{\varsigma,\mathbf{p},\lambda} = \epsilon_{\varsigma,\mathbf{p},\lambda}^\mathrm{D} + \epsilon_{\varsigma,\mathbf{p},\lambda}^\mathrm{TW}, \quad (17a)$$
$$\epsilon_{\varsigma,\mathbf{p},\lambda}^\mathrm{D} = \lambda v_\mathrm{D} p, \quad (17b)$$
$$\epsilon_{\varsigma,\mathbf{p},\lambda}^\mathrm{TW} = -\lambda\varsigma \frac{v_\mathrm{D} a p^2}{4} \cos 3\theta_\mathbf{p} \quad (17c)$$

with $\lambda, \varsigma = \pm 1$. The corresponding isoenergetic contours are shown in Fig. 2.

For low-energy fermions, the unitary transformation from the four-component spinor $\Psi_{\mathbf{p},s}$ to a diagonal electron-hole basis reads as

$$\begin{pmatrix} a_{+,\mathbf{p},s} \\ b_{+,\mathbf{p},s} \\ b_{-,\mathbf{p},s} \\ a_{-,\mathbf{p},s} \end{pmatrix} = \frac{1}{\sqrt{2}} \begin{pmatrix} -g_+(\mathbf{p}) & g_+(\mathbf{p}) & 0 & 0 \\ 1 & 1 & 0 & 0 \\ 0 & 0 & g_-(\mathbf{p}) & -g_-(\mathbf{p}) \\ 0 & 0 & 1 & 1 \end{pmatrix} \cdot \begin{pmatrix} \beta_{+,\mathbf{p},s} \\ \alpha_{+,\mathbf{p},s} \\ \beta_{-,\mathbf{p},s} \\ \alpha_{-,\mathbf{p},s} \end{pmatrix}, \tag{18}$$

where $g_+(\mathbf{k}) = \Phi_{+,\mathbf{k}}/|\Phi_{+,\mathbf{k}}|$, $g_-(\mathbf{k}) = |\Phi_{-,\mathbf{k}}|/\Phi_{-,\mathbf{k}}$, and $\alpha_{\varsigma,\mathbf{p},s}(\beta_{\varsigma,\mathbf{p},s})$ denotes the annihilation operator for an electron (hole) in the conduction (valence) band located near the K_ς point. To linear order in pa, $g_\varsigma(\mathbf{p})$ is given by

$$g_\varsigma(\mathbf{p}) = e^{-i\theta_\mathbf{p}}\left(1 - \frac{i}{4}\varsigma pa \sin 3\theta_\mathbf{p}\right), \tag{19}$$

where $\theta_\mathbf{p}$ is the azimuthal angle of $\mathbf{p}$. The Hamiltonian in the electron-hole basis is the same as in Eq. (15a), except for now the electron and hole operators carry the valley index:

$$H_0 = \sum_{\varsigma,\mathbf{k},s} (\epsilon_{\varsigma,\mathbf{k},+} - \mu)\alpha^\dagger_{\varsigma,\mathbf{k},s}\alpha_{\varsigma,\mathbf{k},s} + (\epsilon_{\varsigma,\mathbf{k},-} - \mu)\beta^\dagger_{\varsigma,\mathbf{k},s}\beta_{\varsigma,\mathbf{k},s}, \tag{20}$$

with $\epsilon_{\varsigma,\mathbf{k},s}$ given by Eq. (17a).

The gradient part of the current operator corresponding to the Hamiltonian in Eqs. (15a)–(15c) is readily found from $\mathbf{J} = -\partial H_0/\partial \mathbf{A}$. The x and y components of $\mathbf{J}$ at $q = 0$ are given by

$$\begin{aligned} J_x &= e\sum_{\mathbf{p},s} \Psi^\dagger_{\mathbf{p},s}\left(v_\mathrm{D}(\tau_z \otimes \sigma_x) - \frac{v_\mathrm{D} a}{2}[p_x(\tau_0 \otimes \sigma_x) - p_y(\tau_0 \otimes \sigma_y)]\right)\Psi_{\mathbf{p},s}, \\ J_y &= e\sum_{\mathbf{p},s} \Psi^\dagger_{\mathbf{p},s}\left(v_\mathrm{D}(\tau_z \otimes \sigma_y) + \frac{v_\mathrm{D} a}{2}[p_y(\tau_0 \otimes \sigma_x) + p_x(\tau_0 \otimes \sigma_y)]\right)\Psi_{\mathbf{p},s}, \end{aligned} \tag{21}$$

where e is the elementary charge.

When expressed in the electron-hole basis, the current operator in Eq. (21) contains both the intraband and interband parts. In a noninteracting doped system, absorption due to intraband transitions is absent, while absorption due to interband ones occurs only for $\omega \geqslant 2\mu$. In an interacting system, absorption due to both intraband and interband transitions occurs already for $\omega \leqslant 2\mu$. For $\omega \ll \mu$, however, the interband contribution is expected to be smaller than the intraband one. As we focus on this range of ω, the interband part of the current will be neglected. Also, the occupied states in the valence band do not contribute to the current. The remaining intraband part of the current is

$$\mathbf{J} = \sum_{\varsigma,\mathbf{p},s} \mathbf{v}_{\varsigma,\mathbf{p}}\alpha^\dagger_{\varsigma,\mathbf{p},s}\alpha_{\varsigma,\mathbf{p},s}, \tag{22}$$

where $\mathbf{v}_{\varsigma,\mathbf{p}} = \nabla\epsilon_{\varsigma,\mathbf{p}}$ is the group velocity at the K_ς point. From now on, band index $\lambda = 1$ will be suppressed.

The density-density interaction between fermions is described by

$$H_\mathrm{int} = 1/2\sum_\mathbf{Q} U_0(\mathbf{Q})\rho_\mathbf{Q}\rho_{-\mathbf{Q}}, \tag{23}$$

where $\rho_\mathbf{Q} = \sum_{\mathbf{p},s}\Psi^\dagger_{\mathbf{p},s}\Psi_{\mathbf{p}+\mathbf{Q},s}$ and $U_0(\mathbf{Q}) = 2\pi e^2/Q$ is the bare Coulomb potential. When expressed in the electron-hole basis, H_int contains a large number of terms, corresponding to interband and intraband, as well as to intervalley and intravalley interactions. Out of those, we will keep only the intra-conduction-band terms, which give the leading contribution to the optical conductivity for $\omega \ll \mu$. Also, we assume that doping is sufficiently low, such that umklapp processes can be neglected. Then, H_int is reduced to

$$\begin{aligned} H_\mathrm{int} = \frac{1}{2}\sum_{\mathbf{k}',\mathbf{p}',\mathbf{k},\mathbf{p}}\sum_{s,s'} & U_0(\mathbf{k}-\mathbf{k}')\delta(\mathbf{k}'+\mathbf{p}'-\mathbf{k}-\mathbf{p}) \\ & \times[\Delta\varphi_{++}(\mathbf{k}',\mathbf{k})\Delta\varphi_{++}(\mathbf{p}',\mathbf{p})\alpha^\dagger_{+,\mathbf{k}',s}\alpha^\dagger_{+,\mathbf{p}',s'}\alpha_{+,\mathbf{p},s'}\alpha_{+,\mathbf{k},s} + \Delta\varphi_{--}(\mathbf{k}',\mathbf{k})\Delta\varphi_{--}(\mathbf{p}',\mathbf{p})\alpha^\dagger_{-,\mathbf{k}',s}\alpha^\dagger_{-,\mathbf{p}',s'}\alpha_{-,\mathbf{p},s'}\alpha_{-,\mathbf{k},s} \\ & + \Delta\varphi_{++}(\mathbf{k}',\mathbf{k})\Delta\varphi_{--}(\mathbf{p}',\mathbf{p})\alpha^\dagger_{+,\mathbf{k}',s}\alpha^\dagger_{-,\mathbf{p}',s'}\alpha_{-,\mathbf{p},s'}\alpha_{+,\mathbf{k},s} + \Delta\varphi_{--}(\mathbf{k}',\mathbf{k})\Delta\varphi_{++}(\mathbf{p}',\mathbf{p})\alpha^\dagger_{-,\mathbf{k}',s}\alpha^\dagger_{+,\mathbf{p}',s'}\alpha_{+,\mathbf{p},s'}\alpha_{-,\mathbf{k},s}] \\ & + U_0(\mathbf{K_0}+\mathbf{k}-\mathbf{k}')[\boldsymbol{\Delta}\varphi_{-+}(\mathbf{k}',\mathbf{k})\boldsymbol{\Delta}\varphi_{+-}(\mathbf{p}',\mathbf{p})\alpha^\dagger_{-,\mathbf{k}',\mathbf{s}}\alpha^\dagger_{+,\mathbf{p}',s'}\alpha_{-,\mathbf{p},s'}\alpha_{+,\mathbf{k},\mathbf{s}} \\ & + \Delta\varphi_{+-}(\mathbf{k}',\mathbf{k})\Delta\varphi_{-+}(\mathbf{p}',\mathbf{k})\alpha^\dagger_{+,\mathbf{k}',s}\alpha^\dagger_{-,\mathbf{p}',s'}\alpha_{+,\mathbf{p},s'}\alpha_{-,\mathbf{k},s}], \end{aligned} \tag{24}$$

where $\Delta\varphi_{\varsigma\varsigma'}(\mathbf{k}',\mathbf{k}) = (1 + e^{-i(\phi_{\varsigma,\mathbf{k}'}-\phi_{\varsigma',\mathbf{k}})})/2$ and $\mathbf{K}_0 = \mathbf{K}_+ - \mathbf{K}_-$ is the vector connecting the valleys. The first two (last four) terms in H_int describe the intravalley (intervalley) interaction. The last two intervalley terms correspond to exchange processes, in which the initial and final states belong to different valleys. Such processes require large momentum transfers, on the order of $K_0 \sim 1/a \gg k_F$, which correspond to small Coulomb matrix elements, and will be neglected. In Sec. III B, it will be shown that the intraband part of the optical conductivity is controlled by processes with small momentum transfers, i.e., $Q \ll k_F$. Therefore, one can also neglect the Q dependence of the phase factors $\Delta\varphi_{\varsigma\varsigma'}(\mathbf{k},\mathbf{Q})$, which are then reduced to $\Delta\varphi_{\varsigma\varsigma'}(\mathbf{k},\mathbf{0}) = 1$. Now $\Delta\varphi_{\varsigma\varsigma'}(\mathbf{k},\mathbf{0})$ does not depend on the valley index, and thus the matrix elements of the intravalley and intervalley interactions are the same. Therefore, we arrive at the final form of the interaction Hamiltonian

$$H_{\rm int} = \frac{1}{2}\sum_{\mathbf{k},\mathbf{p},\mathbf{Q},s,s',\varsigma,\varsigma'} U_0(\mathbf{Q})\alpha^\dagger_{\varsigma,\mathbf{k}+\mathbf{Q},s}\alpha^\dagger_{\varsigma',\mathbf{p}-\mathbf{Q},s'}\alpha_{\varsigma',\mathbf{p},s'}\alpha_{\varsigma,\mathbf{k},s}, \quad (25)$$

in which the valley index plays the role of a (conserved) isospin.

III. OPTICAL CONDUCTIVITY OF A NON-GALILEAN-INVARIANT SYSTEM

A. Formalism

We are interested in the optical conductivity measured in a response to a uniform electric field, which oscillates with frequency ω. In lieu of using the diagrammatic technique for the Kubo formula, we employ the formalism similar to that used in the memory matrix theory [45]. This formalism allows one to obtain directly the real part of the optical conductivity in the ballistic regime, i.e., for $\omega \gg 1/\tau_J(\omega,T)$.

The optical conductivity tensor is given by

$$\sigma_{\ell m}(\omega,T) = \frac{i}{\omega}[\Pi_{\ell m}(\omega,T) - \Pi_{\ell m}(0,T)], \quad (26)$$

where $\Pi_{\ell m}(\omega,T)$ is the current-current correlation function

$$\Pi_{\ell m}(\omega,T) = -i\int_0^\infty dt\, e^{i\omega t}\langle[J_\ell(t),J_m(0)]\rangle \equiv -i\langle[J_\ell,J_m)]\rangle_\omega, \quad (27)$$

where $\ell, m \in \{x,y\}$. The $\Pi_{\ell m}(0,T)$ term in Eq. (26) accounts for the diamagnetic part of the current, which must cancel the gradient part at $\omega = 0$ to maintain gauge invariance [25,48]. Since $\Pi_{\ell m}(0,T)$ is purely real, it contributes only to the imaginary part of the conductivity, whereas its real part is given by

$$\mathrm{Re}\sigma_{\ell m}(\omega,T) = -\frac{1}{\omega}\mathrm{Im}\Pi_{\ell m}(\omega,T). \quad (28)$$

To obtain $\mathrm{Re}\sigma_{\ell m}(\omega,T)$ to lowest order in the interaction, we integrate by parts in Eq. (27) to find

$$\mathrm{Re}\sigma_{\ell m}(\omega,T) = \frac{1}{\omega^3}\langle[\partial_t J_\ell, \partial_t J_m]\rangle_\omega, \quad (29)$$

where $\partial_t\mathbf{J} = \mathrm{i}[H,\mathbf{J}(t)]$. If the Hamiltonian is projected onto the upper Dirac cone, its free part commutes with the current, therefore, $\partial_t\mathbf{J}$ is linear in the interaction [see Eq. (30) below]. If we then average $[\partial_t J_\ell, \partial_t J_m]$ over the noninteracting ground state, the resultant conductivity will be to second order in the interaction. The result obtained in this way is equivalent to evaluating the one-loop diagrams for the Kubo formula, but it eliminates the need for collecting contributions from different diagrams, which partially cancel each other. A similar method was used in Ref. [49] to calculate the conductivity of a Galilean-invariant FL at finite q.

Calculating the commutator of $H_{\rm int}$ and $\mathbf{J}$, we find the time derivative of $\mathbf{J}$ as

$$\partial_t\mathbf{J} = e\frac{i}{2}\sum_{\varsigma\varsigma'}\sum_{\mathbf{kpk'p'}}\sum_{ss'}U(\mathbf{k}-\mathbf{k}')\Delta\mathbf{v}_{\varsigma,\varsigma'} \times \alpha^\dagger_{\varsigma,\mathbf{k}',s}\alpha^\dagger_{\varsigma',\mathbf{p}',s'}\alpha_{\varsigma',\mathbf{p},s'}\alpha_{\varsigma,\mathbf{k},s}\delta(\mathbf{k}'+\mathbf{p}'-\mathbf{k}-\mathbf{p}), \quad (30)$$

where

$$\Delta\mathbf{v}_{\varsigma,\varsigma'} = \mathbf{v}_{\varsigma,\mathbf{k}} + \mathbf{v}_{\varsigma',\mathbf{p}} - \mathbf{v}_{\varsigma,\mathbf{k}'} - \mathbf{v}_{\varsigma',\mathbf{p}'} \quad (31)$$

is a change in the velocity due to an ee collision. To be specific, we take the interaction to be a screened Coulomb potential $U(\mathbf{Q}) = 2\pi e^2/(Q+\kappa)$ where $\mathbf{Q} = \mathbf{k}-\mathbf{k}' = \mathbf{p}'-\mathbf{p}$ with $\kappa = 4e^2\mu/v_D^2$. It will be shown in Sec. III B, however, the scaling form of the conductivity is valid for any form of the interaction, as long $U(\mathbf{Q}\to 0) = \mathrm{const}$ and $U(\mathbf{Q}\to\infty) = 0$. Using Eqs. (30) and (29), we obtain the optical conductivity $\sigma = (\sigma_{xx}+\sigma_{yy})/2$ as

$$\mathrm{Re}\sigma(\omega,T) = e^2\frac{\pi}{\omega^3}(1-e^{-\beta\omega})\sum_{\varsigma\varsigma'}\int\frac{d^Dk'}{(2\pi)^D}\int\frac{d^Dp'}{(2\pi)^D}\int\frac{d^Dk}{(2\pi)^D}\int\frac{d^Dp}{(2\pi)^D}(\Delta\mathbf{v}_{\varsigma,\varsigma'})^2 \times U(\mathbf{k}-\mathbf{k}')\left[U(\mathbf{k}-\mathbf{k}') - \delta_{\varsigma\varsigma'}\frac{U(\mathbf{p}-\mathbf{k}')}{2}\right] \times n_F(\epsilon_{\varsigma,\mathbf{k}'})n_F(\epsilon_{\varsigma',\mathbf{p}'})[1-n_F(\epsilon_{\varsigma,\mathbf{k}})][1-n_F(\epsilon_{\varsigma',\mathbf{p}})]\delta(\omega+\epsilon_{\varsigma',\mathbf{p}'}+\epsilon_{\varsigma,\mathbf{k}'}-\epsilon_{\varsigma,\mathbf{k}}-\epsilon_{\varsigma',\mathbf{p}})\delta(\mathbf{k}'+\mathbf{p}'-\mathbf{k}-\mathbf{p}), \quad (32)$$

where $n_F(\epsilon)$ is the Fermi function and $\beta = 1/T$. A detailed derivation of Eq. (32) is given in Appendix A. The square brackets in the second line of Eq. (32) contain the interaction potential at small and large momentum transfers, given by the first and second terms, respectively. Assuming that typical momentum transfers are small, $Q \ll k_F$, we neglect the second term in the square brackets. It is convenient to introduce the momentum and energy transfers as $\mathbf{Q} = \mathbf{k} - \mathbf{k}' = \mathbf{p}' - \mathbf{p}$ and $\Omega = \epsilon_{\varsigma,\mathbf{k}-\mathbf{Q}} - \epsilon_{\varsigma,\mathbf{k}} = \epsilon_{\varsigma',\mathbf{p}} - \epsilon_{\varsigma',\mathbf{p}+\mathbf{Q}} - \omega$, respectively, upon which Eq. (32) becomes

$$\mathrm{Re}\sigma(\omega, T) = e^2\frac{\pi}{\omega^3}(1-e^{-\beta\omega})\sum_{\varsigma\varsigma'}\int\frac{d^DQ}{(2\pi)^D}\int\frac{d^Dk}{(2\pi)^D}\int\frac{d^Dp}{(2\pi)^D}\int d\Omega(\Delta\mathbf{v}_{\varsigma,\varsigma'})^2U^2(\mathbf{Q})n_\mathrm{F}(\epsilon_{\varsigma,\mathbf{k}}+\Omega)n_\mathrm{F}(\epsilon_{\varsigma',\mathbf{p}}-\omega-\Omega)$$
$$\times[1-n_\mathrm{F}(\epsilon_{\varsigma,\mathbf{k}})][1-n_\mathrm{F}(\epsilon_{\varsigma',\mathbf{p}})]\delta(\Omega-\epsilon_{\varsigma,\mathbf{k}-\mathbf{Q}}+\epsilon_{\varsigma,\mathbf{k}})\delta(\omega+\Omega+\epsilon_{\varsigma',\mathbf{p}+\mathbf{Q}}-\epsilon_{\varsigma',\mathbf{p}}). \tag{33}$$

For a Galilean-invariant system, $\mathbf{v}_\mathbf{k} = \mathbf{k}/m$ and $\Delta\mathbf{v}$ vanishes by momentum conservation, so $\mathrm{Re}\sigma = 0$ for any finite ω. For a non-Galilean-invariant system, $\mathbf{v}_\mathbf{k} \neq \mathbf{k}/m$ and $\Delta\mathbf{v}$ does not vanish exactly, so in general $\mathrm{Re}\sigma \neq 0$. Now, we will discuss the optical conductivity for the particular cases of doped graphene with and without trigonal warping.

B. Monolayer graphene without trigonal warping

In this section, we calculate the optical conductivity of doped graphene without taking trigonal warping into account. In this approximation, the dispersion is isotropic and linear in momentum, the K_+ and K_- valleys are degenerate, and summation over the valley indices in Eq. (33) simply gives a factor of 4. In the rest of this section, the valley index will be suppressed. Equation (33) then becomes

$$\mathrm{Re}\sigma(\omega, T) = e^2\frac{4\pi}{\omega^3}(1-e^{-\beta\omega})\int\frac{d^2Q}{(2\pi)^2}\int\frac{d^2k}{(2\pi)^2}\int\frac{d^2p}{(2\pi)^D}\int d\Omega(\Delta\mathbf{v})^2U^2(\mathbf{Q})$$
$$\times n_\mathrm{F}(\epsilon_\mathbf{k}+\Omega)n_\mathrm{F}(\epsilon_\mathbf{p}-\omega-\Omega)[1-n_\mathrm{F}(\epsilon_\mathbf{k})][1-n_\mathrm{F}(\epsilon_\mathbf{p})]\delta(\Omega-\epsilon_{\mathbf{k}-\mathbf{Q}}+\epsilon_\mathbf{k})\delta(\omega+\Omega+\epsilon_{\mathbf{p}+\mathbf{Q}}-\epsilon_\mathbf{p}). \tag{34}$$

For any isotropic dispersion $\epsilon_\mathbf{k} = \epsilon(k)$, the group velocity can be written as $\mathbf{v}_\mathbf{k} = f(k)\mathbf{k}$, where $f(k) = \epsilon'(k)/k$. Therefore, if we project electrons onto the FS, i.e., put $|\mathbf{k}| = |\mathbf{p}| = |\mathbf{k}-\mathbf{Q}| = |\mathbf{p}+\mathbf{Q}| = k_\mathrm{F}$, then $\Delta\mathbf{v} = 0$. To obtain a nonzero result, one needs to expand the velocity to first order in the deviation from the FS. Writing $k = k_\mathrm{F} + (\epsilon_\mathbf{k} - \mu)/v_\mathrm{F}$ with $v_\mathrm{F} = \epsilon'(k_\mathrm{F})$ (and the same for other momenta), and expanding $\Delta\mathbf{v}$ to first order in $\epsilon_\mathbf{k} - \mu$, we obtain

$$\Delta\mathbf{v} = \frac{w}{k_\mathrm{F}}\bigg[\hat{\mathbf{k}}(\epsilon_{\mathbf{k}-\mathbf{Q}}-\epsilon_\mathbf{k}) + \hat{\mathbf{p}}(\epsilon_{\mathbf{p}+\mathbf{Q}}-\epsilon_\mathbf{p}) + \frac{\mathbf{Q}}{k_\mathrm{F}}(\epsilon_{\mathbf{p}+\mathbf{Q}}-\epsilon_{\mathbf{k}-\mathbf{Q}})\bigg], \tag{35}$$

where $\hat{k} = \mathbf{k}/k$, $\hat{\mathbf{p}} = \mathbf{p}/p$, and

$$w = -\frac{k_\mathrm{F}^2 f'(k_\mathrm{F})}{v_\mathrm{F}} \tag{36}$$

is the dimensionless coefficient which quantifies a deviation from Galilean invariance. Defining two effective masses as $m^* = k_\mathrm{F}/\epsilon'(k_\mathrm{F})$ and $1/\bar{m} = \epsilon''(k_\mathrm{F})$, w can be written as

$$w = 1 - \frac{\bar{m}}{m^*}. \tag{37}$$

For a power-law dispersion $\epsilon(k) \propto k^a$,

$$w = 2 - a. \tag{38}$$

The $a = 2$ case corresponds to a Galilean-invariant system, when $w = 0$ and thus $\mathrm{Re}\sigma(\omega, T) = 0$, as it should be. However, $\mathrm{Re}\sigma(\omega, T) \neq 0$ for any other a. If the dispersion deviates from the quadratic one by a small amount, $\delta\epsilon(k)$, then

$$w = \frac{\delta\epsilon'(k_\mathrm{F})}{v_\mathrm{F}} - m\delta\epsilon''(k_\mathrm{F}), \tag{39}$$

where v_F and m are the Fermi velocity and mass of the quadratic dispersion, respectively.

We will see later on in this section that the integral over Q is logarithmically divergent at the lower limit. This implies that typical $Q \ll k_\mathrm{F}$ and, therefore, the last term in Eq. (35) can be neglected compared to the first two. It is also convenient to express the differences of the dispersion in Eq. (35) via the frequency of light ω and energy transfer Ω using the conservation of energy, as specified by the delta functions in Eq. (33). Restricting now to the Dirac spectrum with $w = 1$, we obtain

$$\Delta\mathbf{v} = \frac{1}{k_\mathrm{F}}\big[\hat{\mathbf{k}}\Omega - \hat{\mathbf{p}}(\Omega+\omega)\big]. \tag{40}$$

We see that $\Delta\mathbf{v}^2 \propto \max\{\omega^2, \Omega^2\}$. This explains the origin of the extra $\max\{T^2, \omega^2\}$ factor in the current relaxation rate, Eq. (6). Since we already obtained $\Delta\mathbf{v}^2$ to leading order in Ω and ω, the remainder of the integrand in Eq. (33) can be projected onto the FS, which amounts to neglecting ω and Ω in the arguments of delta functions. Accordingly,

$$\mathrm{Re}\sigma(\omega, T) = e^2\frac{4\pi N_\mathrm{F}^2}{\omega^3}(1-e^{-\beta\omega})\int\frac{d^2Q}{(2\pi)^2}\int d\epsilon_\mathbf{k}\int d\epsilon_\mathbf{p}\int d\Omega\int_0^{2\pi}\frac{d\theta_{\mathbf{kQ}}}{2\pi}\int_0^{2\pi}\frac{d\theta_{\mathbf{pQ}}}{2\pi}U^2(\mathbf{Q})\Delta\mathbf{v}^2$$
$$\times\, n_\mathrm{F}(\epsilon_\mathbf{k}+\Omega)n_\mathrm{F}(\epsilon_\mathbf{p}-\omega-\Omega)[1-n_\mathrm{F}(\epsilon_\mathbf{k})][1-n_\mathrm{F}(\epsilon_\mathbf{p})]\delta(\epsilon_{\mathbf{p}+\mathbf{Q}}-\epsilon_\mathbf{p})\delta(\epsilon_\mathbf{k}-\epsilon_{\mathbf{k}-\mathbf{Q}}), \tag{41}$$

where $N_F = \mu/2\pi v_D^2$ is the density of states at the Fermi level per spin and per valley, and $\theta_{\mathbf{nn}'}$ is the angle between vectors $\mathbf{n}$ and $\mathbf{n}'$. Next, the dispersions in the delta functions can be expanded to linear order in Q. This imposes kinematic constraints on the angles between $\mathbf{k}$ and $\mathbf{Q}$, and between $\mathbf{p}$ and $\mathbf{Q}$, namely, $\theta_{\mathbf{kQ}} = \pm\pi/2$ and $\theta_{\mathbf{pQ}} = \pm\pi/2$. The first constraint corresponds to the Cooper channel, with $\mathbf{p} = -\mathbf{k}$, while the second one to the collinear channel, with $\mathbf{p} = \mathbf{k}$. Accounting for both of these constraints, we obtain

$$\Delta\mathbf{v}^2 = \frac{2}{k_F^2}[(2\Omega + \omega)^2 + \omega^2]. \tag{42}$$

Now the integrals over $\epsilon_{\mathbf{k}}$, $\epsilon_{\mathbf{p}}$, and Ω in Eq. (41) can be carried out; as shown in Appendix B, the result is

$$\int d\epsilon_{\mathbf{k}} \int d\epsilon_{\mathbf{p}} \int d\Omega[(2\Omega + \omega)^2 + \omega^2] \times n_F(\epsilon_{\mathbf{k}} + \Omega)n_F(\epsilon_{\mathbf{p}} - \omega - \Omega)[1 - n_F(\epsilon_{\mathbf{k}})][1 - n_F(\epsilon_{\mathbf{p}})] = \frac{\omega^5}{15(1 - e^{-\beta\omega})}\left(1 + \frac{4\pi T^2}{\omega^2}\right)\left(3 + \frac{8\pi^4 T^4}{\omega^4}\right). \tag{43}$$

The integral over Q in the leading-logarithm approximation is given by

$$\int_{\max\{|\omega|,T\}/v_D}^{\infty} \frac{dQ}{Q(Q+\kappa)^2} \approx \frac{1}{\kappa^2} \ln \frac{v_D\kappa}{\max(|\omega|, T)}. \tag{44}$$

The logarithmic divergence of the integral above is *a posteriori* justification for neglecting the term proportional to Q in Eq. (35). Collecting everything together, we obtain the final result for the conductivity

$$\mathrm{Re}\sigma(\omega, T) = \frac{e^2}{240\pi^2}\frac{\omega^2}{\mu^2}\left(1 + \frac{4\pi^2 T^2}{\omega^2}\right)\left(3 + \frac{8\pi^2 T^2}{\omega^2}\right) \times \ln \frac{\Lambda_Q}{\max\{|\omega|, T\}}, \tag{45}$$

where $\Lambda_Q = v_D\kappa$. Equation (45) obviously satisfies the first Matsubara-frequency rule [12], i.e., $\mathrm{Re}\sigma(\pm 2\pi iT, T) = 0$. The scaling form in Eq. (45) applies not only to a graphene monolayer with Coulomb interaction, but to any 2D system with an isotropic but nonparabolic dispersion. A change in the dispersion brings in only an overall factor of w^2, defined in Eq. (37), while a change in the interaction affects only the choice of cutoff Λ_Q under the logarithm.

The presence of the logarithmic factor in Eq. (45) is quite interesting by itself. It is well known that the quasiparticle scattering rate in a 2D FL scales as $E^2 \ln E$, where $E = \max\{|\omega|, T\}$ (Refs. [50,51]), but it is also understood that the logarithmic factor comes from processes with small momentum transfers. Therefore, if a E^2 term in the conductivity is allowed due to broken Galilean invariance, it comes without an extra logarithmic factor because the logarithmic singularity is canceled by the "transport factor" $\Delta\mathbf{v}^2$, which is proportional to Q^2 at small Q (Ref. [12]). In our case, however, Galilean invariance is broken only partially, and only a subleading, E^4 term is allowed in the conductivity. One can view this term as resulting from expanding each of the delta functions in Eq. (41) in ω/Q. The two extra factors of ω change the scaling from E^2 to E^4, but the $1/Q^2$ factor results in an additional logarithmic term. Another example of such a behavior is a $T^4 \ln T$ scaling of the conductivity of a Galilean-invariant system with energy-dependent impurity scattering time [2]. Once the logarithmic singularity is present, the coupling constant of the Coulomb interaction enters only via a cutoff because the screened Coulomb potential at $Q \ll \kappa$ does not contain the electron charge.

The current relaxation rate in a conventional FL [Eq. (5)] is related to the quasiparticle lifetime which, in its turn, is related to the electron self-energy via

$$1/\tau_{SP}(\varepsilon, T) = -2\,\mathrm{Im}\Sigma(\varepsilon, T) \propto \varepsilon^2 + \pi^2 T^2. \tag{46}$$

The difference between the scaling forms of $\tau_J(\omega, T)$ in Eq. (5) and $\tau_{SP}(\varepsilon, T)$ in Eq. (46) is due to thermal averaging of (46) over ε. The correct scaling form of $\tau_J(\omega, T)$ can already be deduced from the single-bubble diagram for the conductivity; other diagrams only modify the overall prefactor [12]. On the contrary, the scaling form of $\tau_J(\omega, T)$ for a DFL [Eq. (6)] is not related to that of $\tau_{SP}(\varepsilon, T)$, even if one takes higher-order terms in the self-energy into account.

C. Monolayer graphene with trigonal warping

In this section, we study the effect of trigonal warping, which leads to anisotropy of the FSs around each of the two Dirac points, and also breaks valley degeneracy. The contribution to the optical conductivity from intravalley scattering in Eq. (33) is given by the $\varsigma = \varsigma'$ terms in the sum, and can be evaluated along the same lines as in Sec. III B. In this case, trigonal warping does not lead to any quantitative changes because the FS remains simply connected and convex [2], and the corresponding current relaxation rate is still quartic in ω and T. On the contrary, scattering between nondegenerate valleys does give rise to quadratic scaling, and it is this scattering that we focus on in this section. Intervalley scattering is described by the $\varsigma \neq \varsigma'$ terms in Eq. (33). A typical scattering process is depicted in Fig. 2. The optical conductivity due to intervalley scattering is given by

$$\mathrm{Re}\sigma^{\mathrm{inter}}(\omega, T) = 2\pi e^2 \frac{(1 - e^{-\beta\omega})}{\omega^3} \int \frac{d^2Q}{(2\pi)^2} \int \frac{d\epsilon_{+,\mathbf{k}}}{2\pi} \int \frac{d\epsilon_{-,\mathbf{p}}}{2\pi} \int d\Omega \oint_{C_+} \frac{d\ell_{\mathbf{k}}}{v_{\mathbf{k}}} \oint_{C_-} \frac{d\ell_{\mathbf{p}}}{v_{\mathbf{p}}} (\mathbf{v}_{+,\mathbf{k-Q}} + \mathbf{v}_{-,\mathbf{p+Q}} - \mathbf{v}_{+,\mathbf{k}} - \mathbf{v}_{-,\mathbf{p}})^2 \times U^2(\mathbf{Q})\, n_F(\epsilon_{+,\mathbf{k}} + \Omega)n_F(\epsilon_{-,\mathbf{p}} - \Omega - \omega)[1 - n_F(\epsilon_{+,\mathbf{k}})][1 - n_F(\epsilon_{-,\mathbf{p}})]\delta(\omega + \Omega + \epsilon_{-,\mathbf{p+Q}} - \epsilon_{-,\mathbf{p}}) \times \delta(\Omega - \epsilon_{+,\mathbf{k-Q}} + \epsilon_{+,\mathbf{k}}), \tag{47}$$

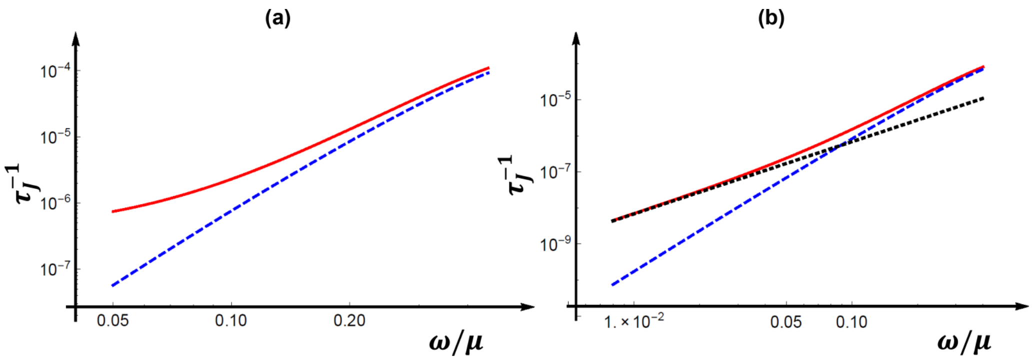

FIG. 3. Solid line: the current relaxation rate $1/\tau_J(\omega, T)$ from Eq. (52) (normalized by μ), as a function of frequency at fixed temperature. Here, $\alpha_e = 0.8$, $k_F a = 0.05$, and $\omega_{TW}/\mu = 0.04$. The dashed and dotted-dashed lines depict the scaling forms for DFL [the first term in Eq. (52)] and conventional FL [the second term in Eq. (52)], respectively. (a) $T/\mu = 10^{-2}$. In this case, the DFL scaling form dominates for all frequencies of interest. (b) $T/\mu = 10^{-4}$. In this case, one can see a crossover between the DFL and conventional FL scaling forms.

where now $\mathbf{k}$ and $\mathbf{p}$ are the initial momenta in the K_+ and K_- valleys, and $d\ell_\mathbf{k}$ ($d\ell_\mathbf{p}$) is the line element of the Fermi contour C_+ (C_-) near K_+ (K_-) point.

A change in the velocity due to an *ee* collision can be written as

$$\mathbf{v}_{+,\mathbf{k}-\mathbf{Q}} + \mathbf{v}_{-,\mathbf{p}+\mathbf{Q}} - \mathbf{v}_{+,\mathbf{k}} - \mathbf{v}_{-,\mathbf{p}} = \Delta\mathbf{v}^{\mathrm{D}} + \Delta\mathbf{v}^{\mathrm{TW}}, \quad (48)$$

where $\Delta\mathbf{v}^{\mathrm{D}}$ and $\Delta\mathbf{v}^{\mathrm{TW}}$ are due to the Dirac and trigonal-warping parts of the velocity, respectively. For electrons on the FS, $\Delta\mathbf{v}^{\mathrm{D}} = 0$, while $\Delta\mathbf{v}^{\mathrm{TW}} \neq 0$. Therefore, the leading-order correction for the conductivity from intervalley scattering is due to $(\Delta\mathbf{v}^{\mathrm{TW}})^2$, and is proportional to a^2. Delegating the computational details to Appendix C, we present here only the final result for the conductivity due to intervalley scattering:

$$\mathrm{Re}\sigma^{\mathrm{inter}}(\omega, T) = \frac{29e^2}{48\pi^2}\alpha_e^2|\ln\alpha_e|(k_F a)^2\left(1 + \frac{4\pi^2T^2}{\omega^2}\right), \quad (49)$$

where

$$\alpha_e = \frac{e^2}{v_D} \quad (50)$$

is the effective fine-structure constant. The ω/T scaling of $\mathrm{Re}\sigma^{\mathrm{inter}}$ is same as for a conventional FL [cf. Eq. (1)] but with a small prefactor of $(k_F a)^2$, which characterizes the strength of trigonal warping.

D. Combined result for the conductivity from intervalley and intervalley scattering

1. High-frequency regime

The total conductivity is given by the sum of the intravalley [Eq. (45)] and intervalley [Eq. (49)] contributions, and can be cast into a Drude-type form

$$\mathrm{Re}\sigma(\omega, T) = \frac{ne^2}{m^*}\frac{1}{\omega^2\tau_J(\omega, T)}, \quad (51)$$

where n is the number density, $m^* = k_F/v_D$ is the effective mass, and the current relaxation time is defined as

$$\frac{1}{\tau_J(\omega, T)} = \frac{1}{240\pi}\frac{(\omega^2 + 4\pi^2T^2)(3\omega^2 + 8\pi^2T^2)}{\mu^3}\ln\frac{\alpha_e\mu}{\max\{|\omega|, T\}} + \frac{29}{48\pi}\alpha_e^2|\ln\alpha_e|(k_F a)^2\frac{\omega^2 + 4\pi^2T^2}{\mu}. \quad (52)$$

The first term in $1/\tau_J$ arises from intravalley scattering and is specific for a DFL, while the second one is a Gurzhi-type contribution arising from intervalley scattering. The competition between the two terms is determined by the hierarchy of the three energy scales: ω, T, and $\omega_{TW} \equiv \alpha_e(k_F a)\mu \ll \mu$. As an example, we analyze the dependence of $1/\tau_J$ on ω at fixed T. If $\omega_{TW} \ll T$, the effect of trigonal warping is negligible: $1/\tau_J$ is mostly given by the DFL term. This behavior is shown in the left panel of Fig. 3(a). If $T \ll \omega_{TW}$, $1/\tau_J$ starts with the T^2 term for $\omega \ll T$, then scales as ω^2 for $T \ll \omega \ll \omega_{TW}$, and finally follows the ω^4 dependence for $\omega_{TW} \ll \omega$. This case is illustrated in Fig. 3(b).

2. Low-frequency regime

Although Eq. (51) looks like a high-frequency tail of the conventional Drude formula $\mathrm{Re}\sigma = e^2 n\tau_J/m(1 + \omega^2\tau_J^2)$, it would be incorrect to extrapolate this result to the *dc* limit because *ee* interaction in the absence of umklapp scattering cannot render the dc conductivity finite [52]. In fact, Eq. (51) is valid only for $\omega \gg 1/\tau_J(0, T)$. In this section, we will show that, in the absence of disorder and at $\omega \to 0$, the conductivity can be described by the sum of a delta-function term and a regular part:

$$\mathrm{Re}\sigma(\omega \to 0, T) = \frac{\pi ne^2}{m^*}\delta(\omega) + \sigma_{\mathrm{reg}}(T), \quad (53)$$

where $\sigma_{\rm reg}(T)$ scales either as T^{-4} or T^{-2}, depending on whether T is higher or lower than $\omega_{\rm TW}$. The form in Eq. (53) pertains to any non-Galilean-invariant system, in which *ee* interaction can render the conductivity finite only at a finite but not zero frequency. For example, this form follows from the semiclassical equations of motion for a two-band system (in this case, the delta-function term is absent if the system is compensated) [3].

On a more general level, Eq. (53) can be derived from the Boltzmann equation, using the method outlined in Ref. [2]. As we are now interested in the limit of $\omega \ll T$, it suffices to consider a semiclassical form of the Boltzmann equation

$$(-i\omega + 0^+)\delta f_{\mathbf{k}} - e(\mathbf{v_k}\cdot\mathbf{E})n'_{\mathbf{k}} = -I_{ee}[\delta f_{\mathbf{k}}], \tag{54}$$

where $\delta f_{\mathbf{k}}$ is a nonequilibrium correction to the Fermi function ($n_{\mathbf{k}}$) and $I_{ee}[\delta f_{\mathbf{k}}]$ is the (linearized) *ee* collision integral. The collision integral can be viewed as a linear operator acting on $\delta f_{\mathbf{k}}$:

$$I_{ee}[\delta f_{\mathbf{k}}] = \sum_{\mathbf{k}'} \hat{I}_{ee}(\mathbf{k},\mathbf{k}')\delta f_{\mathbf{k}'}. \tag{55}$$

In general, $\hat{I}_{ee}$ is non-Hermitian and thus can be written as a direct product of its left (L) and right (R) eigenvectors

$$\hat{I}_{ee} = \frac{1}{\tau^*_{ee}(T)}\sum_n \xi_n |\Phi^n_R\rangle\langle\Phi^n_L|, \tag{56}$$

where ξ_n is the nth eigenvalue and $\tau^*_{ee}(T)$ is the effective *ee* scattering time, which defines the magnitude of $\hat{I}_{ee}$. Without a loss of generality, we can choose $\tau^*_{ee}(T)$ to coincide with $\tau_J(0,T)$ given by Eq. (52), i.e.,

$$\frac{1}{\tau^*_{ee}(T)} = \frac{1}{\tau_J(0,T)} = \frac{2\pi^3}{15}\frac{T^4}{\mu^3}\ln\frac{\alpha_{\rm e}\mu}{T}, \tag{57}$$

where for brevity we omitted the T^2 term resulting from trigonal warping. Because Φ^n_L and Φ^n_R form an orthonormal basis, a general solution of Eq. (54) can be written as

$$\delta f_{\mathbf{k}} = \sum_n c_n |\Phi^n_R\rangle. \tag{58}$$

Substituting this expansion into Eq. (54), we obtain coefficients c_n as

$$c_n = \frac{e\langle\Phi^n_L|\mathbf{v_k}\cdot\mathbf{E}n'_{\mathbf{k}}\rangle}{-i\omega + \frac{\xi_n}{\tau^*_{ee}(T)} + 0^+}. \tag{59}$$

If *ee* interaction conserves momentum, I_{ee} is nullified by a combination $\mathbf{A}\cdot\mathbf{k}$, where $\mathbf{A}$ is an arbitrary $\mathbf{k}$-independent vector [52]. This means that operator $\hat{I}_{ee}$ has a zero mode with eigenvalue $\xi_0 = 0$. In the limit of $\omega\tau^*_{ee}(T)\to 0$, the series in Eq. (58) contains only the zero-mode term with

$$c_0 = \frac{e\langle\Phi^0_L|\mathbf{v_k}\cdot\mathbf{E}n'_{\mathbf{k}}\rangle}{-i\omega + 0^+}. \tag{60}$$

The corresponding contribution to $\delta f_{\mathbf{k}}$ gives the delta-function term in Eq. (53). The next-to-leading contribution corresponds to the minimum nonzero eigenvalue $\xi_1 > 0$:

$$c_1 = \frac{e\langle\Phi^1_L|\mathbf{v_k}\cdot\mathbf{E}n'_{\mathbf{k}}\rangle}{-i\omega + \frac{\xi_1}{\tau^*_{ee}(T)} + 0^+}. \tag{61}$$

Because ξ_n are the eigenvalues of a dimensionless operator, which does not contain any physical parameters, we should expect that $\xi_1 \sim 1$. For $\omega \ll 1/\tau^*_{ee}$, one can then neglect ω in the denominator of c_1. The corresponding contribution to $\delta f_{\mathbf{k}}$ gives the second term in Eq. (53).

So far, we have found the asymptotic forms of the conductivity in the opposite limits of $\omega \gg 1/\tau_J(0,T)$ and $\omega \ll 1/\tau_J(0,T)$, given by Eqs. (51) and (53), respectively. Although Eq. (51) matches in order of magnitude with $\sigma_{\rm reg}$ in Eq. (53) at $\omega \sim 1/\tau_J(0,T)$, it does not mean that $\sigma_{\rm reg}$ can be described by the Drude form at all frequencies. A precise form of ${\rm Re}\,\sigma(\omega,T)$ in the intermediate range of $\omega \sim 1/\tau_J(0,T)$ can be obtained only by an exact solution of the Boltzmann equation, which is outside the scope of this paper.

IV. DIRAC-FERMI LIQUID WITH IMPURITIES

In this section, we consider an interplay between impurity and *ee* scattering in a DFL at the level of the semiclassical Boltzmann equation, which neglects quantum interference and hydrodynamic effects. We assume that the effective impurity radius is much smaller than the Fermi wavelength but much larger than the lattice spacing. In this case, impurities act as pointlike, isotropic scatterers for electrons within the K_+ and K_- valleys, while scattering between the valleys is suppressed. As in the previous sections, we assume that *ee* interaction is long ranged and also neglect trigonal warping, such that the valley degree of freedom plays the role of conserved isospin. The nonequilibrium correction to the Fermi function can be parametrized as $\delta f_{\mathbf{k}} = -Tn'_{\mathbf{k}}g_{\mathbf{k}}$. Then, the linearized Boltzmann equation reads as

$$-\left(i\omega - \frac{1}{\tau_i}\right)Tn'_{\mathbf{k}}g_{\mathbf{k}} - e\mathbf{E}\cdot\mathbf{v_k}n'_{\mathbf{k}} = -I_{ee}[g_{\mathbf{k}}], \tag{62}$$

where τ_i is the transport mean-free time for impurity scattering and

$$\begin{aligned} I_{ee}[g_{\mathbf{k}}] = \int\frac{d^2\mathbf{k}'}{(2\pi)^2}\int\frac{d^2\mathbf{p}'}{(2\pi)^2}\int\frac{d^2\mathbf{p}}{(2\pi)^2}W_{\mathbf{k},\mathbf{p};\mathbf{k}',\mathbf{p}'} \\ \times(g_{\mathbf{k}} + g_{\mathbf{p}} - g_{\mathbf{k}'} - g_{\mathbf{p}'}) \\ \times n_{\mathbf{k}}n_{\mathbf{p}}(1-n_{\mathbf{k}'})(1-n_{\mathbf{p}'}) \\ \times\delta(\epsilon_{\mathbf{k}} + \epsilon_{\mathbf{p}} - \epsilon_{\mathbf{k}'} - \epsilon_{\mathbf{p}'})\delta(\mathbf{k}+\mathbf{p}-\mathbf{k}'-\mathbf{p}'). \end{aligned} \tag{63}$$

With spin and valley degeneracy taken into account [52,53], the scattering probability to lowest order in an instantaneous interaction is given by

$$W_{\mathbf{k},\mathbf{p};\mathbf{k}',\mathbf{p}'} = 8\pi U(\mathbf{k}-\mathbf{k}')\big[U(\mathbf{k}-\mathbf{k}') - \tfrac{1}{2}U(\mathbf{k}-\mathbf{p}')\big], \tag{64}$$

where the first (second) term in the square brackets comes from direct (exchange) *ee* interaction. In our model of a weakly screened Coulomb potential, the exchange term can be neglected and

$$W_{\mathbf{k},\mathbf{p};\mathbf{k}',\mathbf{p}'} = 8\pi U^2(\mathbf{k}-\mathbf{k}'). \tag{65}$$

A. Low temperatures: Slow electron-electron scattering

We now solve Eq. (62) for the case of low temperatures, when *ee* collisions are less frequent than *ei* collisions, and the *ee* contribution can be evaluated perturbatively in I_{ee}; cf.

Refs. [2,9,54]. At the first step, we solve Eq. (62) with $I_{ee} = 0$, which yields

$$g_{\mathbf{k}}^{(0)} = -\frac{e\tau_i(\mathbf{v_k}\cdot\mathbf{E})}{T(1-i\omega\tau_i)} \quad (66)$$

and the corresponding contribution to the optical conductivity is of the Drude form

$$\sigma_i(\omega) = \frac{e^2 n\tau_i}{m^*(1-i\omega\tau_i)}. \quad (67)$$

Next, we substitute $g_{\mathbf{k}}^{(0)}$ back into Eq. (62) and find a correction due to *ee* scattering

$$g_{\mathbf{k}}^{(1)} = \frac{\tau_i}{T(1-i\omega\tau_i)n'_{\mathbf{k}}} I_{ee}\big[g_{\mathbf{k}}^{(0)}\big]. \quad (68)$$

The corresponding correction to the optical conductivity is given by

$$\begin{aligned}\delta\sigma_{ee} = &-\frac{4\pi e^2\tau_i^2 N_{\rm F}^2}{T(1-i\omega\tau_i)^2}\int\frac{d^2Q}{(2\pi)^2}\int d\epsilon_{\mathbf{k}}\int d\epsilon_{\mathbf{p}}\int d\Omega\\ &\times\int\frac{d\theta_{\mathbf{k}}}{2\pi}\int\frac{d\theta_{\mathbf{p}}}{2\pi}(\Delta\mathbf{v})^2U^2(\mathbf{Q})\\ &\times n(\epsilon_{\mathbf{k}})n(\epsilon_{\mathbf{p}})[1-n(\epsilon_{\mathbf{k}}+\Omega)][1-n(\epsilon_{\mathbf{p}}-\Omega)]\\ &\times\delta(\epsilon_{\mathbf{k}}-\epsilon_{\mathbf{k-Q}}+\Omega)\delta(\epsilon_{\mathbf{p}}-\epsilon_{\mathbf{p+Q}}-\Omega), \end{aligned} \quad (69)$$

where, as before, $\Delta\mathbf{v} = \mathbf{v_k}+\mathbf{v_p}-\mathbf{v_{k-Q}}-\mathbf{v_{p+Q}}$. Note that the integral in the last equation is the same as in Eq. (34) but with $\omega = 0$ and, therefore, the rest of the calculation is the same as in Sec. III B. The final result reads as

$$\delta\sigma_{ee}(\omega, T) = -\frac{e^2 n\tau_i}{m^*}\frac{1-\omega^2\tau_i^2}{(1-i\omega\tau_i)^2}\frac{\tau_i}{\tau_{ee}^*(T)}, \quad (70)$$

where $\tau_{ee}^*(T)$ is given by Eq. (57). Note that Eq. (70) can be obtained by replacing τ_i in the Drude formula [Eq. (67)] by the effective scattering time $\tau_{\rm eff}(T) = \tau_i\tau_{ee}^*(T)/[\tau_i + \tau_{ee}^*(T)]$, and expanding the result to first order in $1/\tau_{ee}^*(T)$. In this regime, therefore, we recover the Mathiessen rule, i.e., the *ei* and *ee* channels act as two resistors connected in series. Correspondingly, the real and imaginary parts of the conductivity are given by

$$\begin{Bmatrix}\mathrm{Re}\sigma(\omega,T)\\ \mathrm{Im}\sigma(\omega,T)\end{Bmatrix} = \frac{e^2 n\tau_{\rm eff}(T)}{m^*\big[1+\omega^2\tau_{\rm eff}^2(T)\big]}\times\begin{Bmatrix}1\\ \omega\tau_{\rm eff}(T)\end{Bmatrix}. \quad (71)$$

B. High temperatures: Fast electron-electron scattering

We now turn to the opposite limit of high temperatures, when *ee* scattering is faster than *ei* one. The analysis of this limit proceeds in the same way as in Sec. III D 2; we only need to replace an infinitesimally small damping term [0^+ in Eq. (54)] by finite $1/\tau_i$. Consequently, Eq. (59) for expansion coefficients c_n is replaced by

$$c_n = \frac{e\big\langle\Phi_L^{\xi}\big|\mathbf{v_k}\cdot\mathbf{E}n'_{\mathbf{k}}\big\rangle}{-i\omega+\tau_i^{-1}+\frac{\xi_n}{\tau_{ee}^*(T)}}. \quad (72)$$

At $1/\tau_{ee}^*(T)\to\infty$, the $\xi_0 = 0$ eigenvalue gives the leading contribution, and the delta-function term in Eq. (53) is replaced by the Drude form with the width given by $1/\tau_i$, as in Eq. (67). This Drude form is completely independent of the *ee* interaction, despite the fact that *ee* scattering is the dominant one. On the other hand, one can neglect $1/\tau_i$ in all $c_{n\neq 0}$. This results in replacing the second, regular term in Eq. (59) by another Drude form with the width given by $1/\tau_{ee}^*(T)$. Correspondingly, the real and imaginary parts of the conductivity are given by

$$\begin{Bmatrix}\mathrm{Re}\sigma(\omega,T)\\ \mathrm{Im}\sigma(\omega,T)\end{Bmatrix} = \frac{ne^2}{m^*}\times\begin{Bmatrix}\frac{\tau_i}{1+\omega^2\tau_i^2}+\frac{\tau_{ee}^*(T)}{1+\omega^2\tau_{ee}^{*2}}\\ \frac{\omega\tau_i^2}{1+\omega^2\tau_i^2}+\frac{\omega\tau_{ee}^{*2}(T)}{1+\omega^2\tau_{ee}^{*2}}\end{Bmatrix}. \quad (73)$$

Physically, it means that if *ee* scattering is faster than *ei* one, the two channels act as two resistors connected in parallel.

C. *dc* limit

The analysis presented in the two preceding sections can be also extended to include the dc limit ($\omega = 0$). In particular, the conductivity in the regime of slow *ee* scattering is found simply by substituting $\omega = 0$ into Eq. (70). Converting the result into the resistivity $\rho(T) = 1/\sigma(0, T)$, we obtain

$$\rho(T) = \rho_{\rm i} + \frac{m^*}{ne^2}\frac{1}{\tau_{ee}^*(T)} \propto \text{const} + O(T^4\ln T), \quad (74)$$

where $\rho_{\rm i} = m^*/ne^2\tau_i$ is the residual resistivity and $\tau_{ee}^*(T)$ is given by Eq. (57). Although it may look as if Eq. (74) obeys the Mathiessen rule, it is only valid for low enough temperatures, when $\tau_{ee}^*(T)\gg\tau_i$ or $T\ll T_i = (\mu^3/\tau_i)^{1/4}$. Note that $1/\tau_i \ll T_i \ll \mu$ as long as the "good-metal condition" $\mu\tau_i\gg 1$ is satisfied.

In the opposite limit of $\tau_{ee}^*(T)\ll\tau_i$ ($T\gg T_i$), *ee* scattering is the dominant mechanism. However, it conserves momentum and thus can only establish a quasiequilibrium state with the Fermi surface displaced by a drift velocity whose magnitude is still controlled by *ei* scattering. The high-temperature limit was analyzed in Ref. [2] using the method outlined in Sec. III D 2. The key ingredient here is again the existence of the zero mode of the *ee* collision integral. Without repeating the analysis here, we simply reproduce here the result of Ref. [2] for the high-T limit of the conductivity

$$\sigma_{\ell m}|_{T\gg T_i} = 2N_v e^2 N_{\rm F}\tau_i\sum_n\frac{\langle v_\ell k_n\rangle\langle v_m k_n\rangle}{\langle k_n^2\rangle}, \quad (75)$$

where N_v is the valley degeneracy (= 4 for graphene) and $\langle\dots\rangle$ denotes averaging over the FS. At the same time, the low-T limit is given by

$$\sigma_{\ell m}|_{T\ll T_i} = 2N_v e^2 N_{\rm F}\tau_i\langle v_\ell v_m\rangle. \quad (76)$$

In general, high- and low-T limits are different. However, for an isotropic dispersion, which is the case of doped graphene without trigonal warping, the two limits coincide. Therefore,

$$\rho(T\gg T_i) = \rho_i[1+O(\tau_{ee}^*/\tau_i)] = \text{const} + O(T^{-4}). \quad (77)$$

In-between the two limits given by Eqs. (74) and (77), the resistivity reaches a maximum of height $\sim\rho_i$ at $T\sim T_i$, as illustrated in Fig. 4.

We emphasize that the maximum in the resistivity occurs in a model which accounts only for the *ei* and *ee* scattering channels. In real systems, scattering by phonon gives rise a monotonically increasing with T resistivity, which may mask

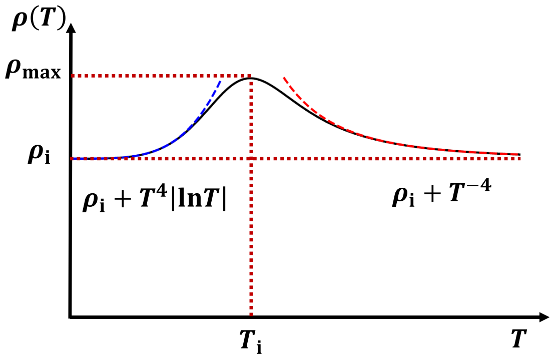

FIG. 4. A sketch of the temperature dependence of the dc resistivity of doped graphene in the presence of electron-impurity and electron-electron scattering. Here, ρ_i is the residual resistivity due to impurities, $\rho_{\max} \sim \rho_i$, $T_i = (\mu^3/\tau_i)^{1/4}$, and τ_i is the transport time for electron-impurity scattering. The dashed lines depict the low- and high-T asymptotic limits.

the maximum. An interplay between electron-electron and electron-phonon scattering is discussed further in Sec. VI D.

V. DYNAMICAL CHARGE SUSCEPTIBILITY OF A DIRAC-FERMI LIQUID

A. Formalism

In this section, we analyze the dissipative part of the charge susceptibility of a DFL, $\text{Im}\chi_c(\mathbf{q}, \omega)$. This quantity can be measured on its own, e.g., via momentum-resolved electron energy-loss spectroscopy (M-EELS) [55–57], and is also related to the longitudinal conductivity via the Einstein relation

$$\text{Re}\sigma(\mathbf{q}, \omega) = \frac{e^2\omega}{q^2}\text{Im}\chi_c^{\text{irr}}(\mathbf{q}, \omega), \tag{78}$$

where the superscript irr denotes the irreducible part. In this section, we will find $\text{Im}\chi_c^{\text{irr}}(\mathbf{q}, \omega)$ from the Kubo formula, to one-loop order in a dynamically screened Coulomb interaction. Equation (78) can then be used as an independent

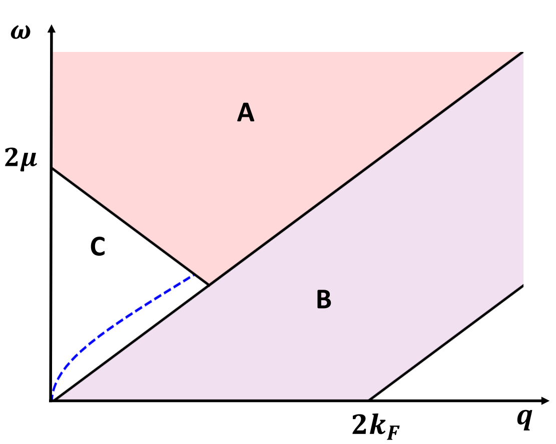

FIG. 5. Regions A and B correspond to particle-hole continua in doped graphene. A nonzero spectral weight in region C is due to the interaction between quasiparticles, described by the diagrams in Fig. 6. The dashed line shows the plasmon dispersion.

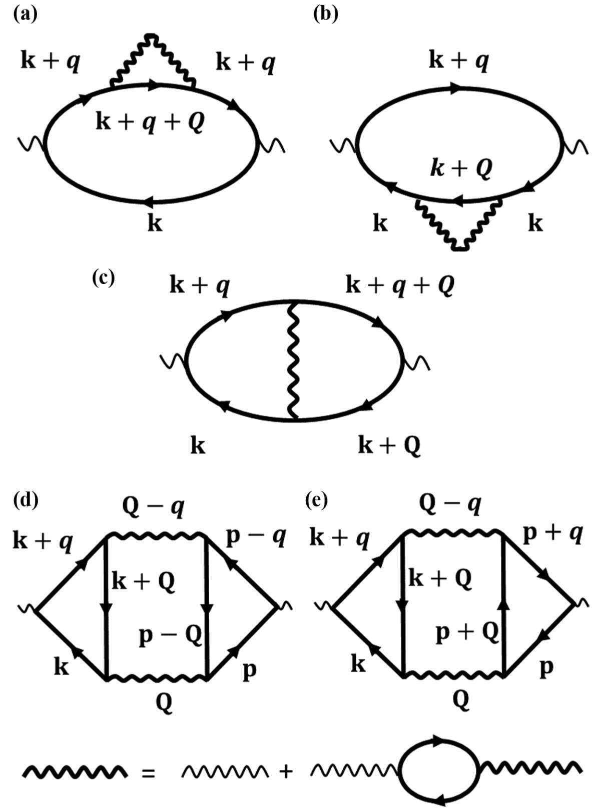

FIG. 6. One-loop diagrams for the irreducible charge susceptibility. The bold wavy line denotes a dynamically screened Coulomb interaction.

check for the result of Sec. III for $\text{Re}\sigma(\mathbf{q}, \omega)$, obtained via the equations of motion and Boltzmann equation.

The continua of particle-hole excitations in doped graphene are shown by the shaded (red and purple) regions in Fig. 5. Within these regions, $\text{Im}\chi_c^{\text{irr}}(\mathbf{q}, \omega) \neq 0$ even for noninteracting electrons. At the level of random phase approximation (RPA), *ee* interaction modifies the spectral weight within the continua but does not lead to a nonzero spectral weight outside the continua. The latter occurs only if the interaction between quasiparticles is taken into account, which means that one has to go beyond RPA and renormalize the polarization bubble by the interaction. One-loop diagrams for the irreducible charge susceptibility are shown in Fig. 6, where the bold wavy line denotes a dynamically screened Coulomb interaction

$$U(\mathbf{Q}, \Omega_l) = \left[U_0^{-1}(\mathbf{Q}) - \Pi(\mathbf{Q}, \Omega_l)\right]^{-1}, \tag{79}$$

$\Pi(\mathbf{Q}, \Omega_l)$ is the free-electron polarization bubble, and $U_0(\mathbf{Q}) = 2\pi e^2/Q$. In what follows, we focus on the case of small-Q scattering, when the phase factors in the matrix elements of spinor wave functions can be replaced by unity. At this level, the information about the Dirac nature of the system enters only via the linear dispersion of electronic excitation and also via the additional (twofold) valley degeneracy.

As in Ref. [58], the contributions from the self-energy and exchange diagrams [Figs. 6(a)–6(c)] can be combined as

$$\chi_c^{(\mathrm{S,E})}(\mathbf{q},\omega_m) = -2\iiint\int \frac{d^2Q\, d^2k\, d\Omega_l d\varepsilon_n}{(2\pi)^6} U(\mathbf{Q},\Omega_l)\frac{(\epsilon_{\mathbf{k+q}}-\epsilon_{\mathbf{k}}-\epsilon_{\mathbf{k+Q+q}}+\epsilon_{\mathbf{k+Q}})^2}{(i\omega_m-\epsilon_{\mathbf{k+Q+q}}+\epsilon_{\mathbf{k+Q}})^2(i\omega_m-\epsilon_{\mathbf{k+q}}+\epsilon_{\mathbf{k}})^2}$$
$$\times[G(\mathbf{k},\varepsilon_n)-G(\mathbf{k}+\mathbf{q},\varepsilon_n+\omega_m)][G(\mathbf{k}+\mathbf{Q},\varepsilon_n+\Omega_l)-G(\mathbf{k}+\mathbf{Q}+\mathbf{q},\varepsilon_n+\Omega_l+\omega_m)], \tag{80}$$

where $G(\mathbf{k},\varepsilon_n)=(i\varepsilon_n-\epsilon_{\mathbf{k}}+\mu)^{-1}$ is the (Matsubara) free-electron Green's function $\epsilon_{\mathbf{k}}=v_{\mathrm{D}}k$. [An overall factor of 2 in Eq. (80) is due to valley degeneracy.] We focus on the range of momenta and frequencies away from both continua boundaries, i.e., on the range $v_{\mathrm{D}}q \ll \omega \ll \mu$ within region C in Fig. 5. To order q^2, Figs. 6(a)–6(c) yield (see Appendix D 1 for details)

$$\mathrm{Im}\,\chi_c^{(\mathrm{S,E})}(\mathbf{q},\omega) = \frac{e^4}{\pi^2 v_{\mathrm{D}}^2}\left[\frac{2}{3}\frac{q^2}{\omega}\int_0^{\Lambda_Q}\frac{dQ\,Q}{(Q+\kappa)^2} - \frac{1}{5}\frac{q^2\omega}{\kappa^2 v_{\mathrm{D}}^2}\ln\frac{v_{\mathrm{D}}\kappa}{|\omega|}\right]. \tag{81}$$

The first term in Eq. (81) is not specific to whether the system is Galilean invariant or not, while the second term is specific for a DFL. For the charge susceptibility, the choice of the upper-limit cutoff (Λ_Q) in the first term is arbitrary because this term cancels out with the corresponding contribution from the Aslamazov-Larkin (AL) diagrams [Figs. 6(d) and 6(e)].[1]

To order q^2, the contribution from the AL diagrams can be written as

$$\chi_c^{(\mathrm{AL})}(\mathbf{q},\omega_m) = 16\iint\frac{d^2Q\,d\Omega_l}{(2\pi)^3}U(\mathbf{Q},\Omega_l)U(\mathbf{Q}-\mathbf{q},\Omega_l-\omega_m)[\mathcal{T}^2(\mathbf{Q},\mathbf{q},\Omega_l,\omega_m)+|\mathcal{T}(\mathbf{Q},\mathbf{q},\Omega_l,\omega_m)|^2], \tag{82}$$

where

$$\mathcal{T}(\mathbf{Q},\mathbf{q},\Omega_l,\omega_m) = \iint\frac{d^2k\,d\varepsilon_n}{(2\pi)^3}G(\mathbf{k},\varepsilon_n)G(\mathbf{k}+\mathbf{q},\varepsilon_n+\omega_m)G(\mathbf{k}+\mathbf{Q},\varepsilon_n+\Omega_l) \tag{83}$$

is a "triangle" formed by three Green's functions. Under the same conditions as for Eq. (81), the AL contribution is reduced to (see Appendix D 2 for details)

$$\mathrm{Im}\,\chi_c^{(\mathrm{AL})}(\mathbf{q},\omega) = \frac{e^4}{\pi^2 v_{\mathrm{D}}^2}\left[-\frac{2}{3}\frac{q^2}{\omega}\int_0^{\Lambda_Q}\frac{dQ\,Q}{(Q+\kappa)^2} + \frac{2}{5}\frac{q^2\omega}{\kappa^2 v_{\mathrm{D}}^2}\ln\frac{v_{\mathrm{D}}\kappa}{|\omega|}\right]. \tag{84}$$

On adding up Eqs. (81) and (84), the first terms in each of the equations cancel each other, and we obtain the total $O(q^2)$ contribution to the charge susceptibility as

$$\mathrm{Im}\,\chi_c^{\mathrm{irr}}(\mathbf{q},\omega) = \frac{q^2\omega}{80\pi^2\mu^2}\ln\frac{v_{\mathrm{D}}\kappa}{|\omega|}. \tag{85}$$

One can see that $\mathrm{Im}\,\chi_c^{\mathrm{irr}}(\mathbf{q},\omega)$ in the equation above and the $T=0$ value of the longitudinal conductivity in Eq. (45) do satisfy the Einstein relation (78).

The $O(q^2)$ result for the charge susceptibility suffices to obtain the $q=0$ limit of the conductivity via the Einstein relation. However, if the goal is to find the charge susceptibility in the entire region C in Fig. 5, one also needs to calculate the $O(q^4)$ term. Such a calculation was performed in Ref. [44], where it was shown that the $O(q^4)$ term in the charge susceptibility behaves as q^4/ω^3. For completeness, we verified this result in a different way: by calculating the conductivity to order q^2 first and then using the Einstein relation. The conductivity was calculated by using the method developed in Ref. [49], in which one extracts the conductivity from the rate of photon absorption by interacting electrons. Deferring the details to a forthcoming publication [59], we present here only the result:

$$\mathrm{Re}\,\sigma(\mathbf{q},\omega) = \frac{e^2}{24\pi^2}\left[\frac{\omega^2}{10\mu^2}\left(1+4\pi^2\frac{T^2}{\omega^2}\right)\left(3+4\pi^2\frac{T^2}{\omega^2}\right)\ln\frac{v_{\mathrm{D}}\kappa}{\max\{|\omega|,2\pi T\}} + \frac{q^2\kappa^2}{m^{*2}\omega^2}\left(1+4\pi^2\frac{T^2}{\omega^2}\right)\ln\frac{k_{\mathrm{F}}}{\kappa}\right]. \tag{86}$$

The first term coincides with the $q=0$ limit of the conductivity in Eq. (45), while the second term is the $O(q^2)$ contribution. Parenthetically, we note that the $O(q^2)$ term is the same as for a Galilean-invariant 2D FL (with $m^*\to k_{\mathrm{F}}/v_{\mathrm{F}}$). In this regard, our result disagrees with that of Ref. [49], where it was argued that in the Galilean-invariant case $\mathrm{Re}\,\sigma = (e^2/12\pi^2)(q^2/k_{\mathrm{F}}^2)(1+4\pi^2T^2/\omega^2)\ln(v_{\mathrm{F}}\kappa/\max\{|\omega|,T\})$. We find that such a term is, indeed, present but is subleading to the $O(q^2)$ term in Eq. (86) for $\omega \ll v_{\mathrm{F}}\kappa$.

Substituting Eq. (86) into the Einstein relation, we obtain the charge susceptibility to order q^4 as

$$\mathrm{Im}\,\chi_c^{\mathrm{irr}}(\mathbf{q},\omega) = \frac{1}{24\pi^2}\left[\frac{q^2\omega}{10\mu^2}\left(1+4\pi^2\frac{T^2}{\omega^2}\right)\left(3+4\pi^2\frac{T^2}{\omega^2}\right)\ln\frac{v_{\mathrm{D}}\kappa}{\max\{|\omega|,2\pi T\}} + \frac{q^4\kappa^2}{m^{*2}\omega^3}\left(1+4\pi^2\frac{T^2}{\omega^2}\right)\ln\frac{k_{\mathrm{F}}}{\kappa}\right]. \tag{87}$$

[1] If we were to calculate the spin susceptibility, however, the AL diagrams would vanish on tracing spins out, and the first term in Eq. (81) would provide the leading contribution. In this case, an appropriate choice would be $\Lambda_Q \sim k_{\mathrm{F}}$.

The $T = 0$ limit of the $O(q^2)$ term in Eq. (87) coincides with our previous result in Eq. (85). At $T = 0$, the $O(q^2)$ and $O(q^4)$ terms in $\mathrm{Im}\chi_c^{\mathrm{irr}}$ become comparable at $\omega \sim \omega_{\mathrm{p}}(q)$, where $\omega_{\mathrm{p}}(q) = 2\sqrt{\mu e^2 q}$ is the plasmon dispersion in graphene. Since the plasmon dispersion lies within region C in Fig. 6, both these terms need to be taken into account.

B. Total charge susceptibility and plasmon damping

We now analyze the imaginary part of the total charge susceptibility, obtained by summing up RPA diagrams with bubbles given by χ_c^{irr}:

$$\mathrm{Im}\chi_c(\mathbf{q},\omega) = \frac{\mathrm{Im}\chi_c^{\mathrm{irr}}(\mathbf{q},\omega)}{\left[1 + U_0(\mathbf{q})\mathrm{Re}\chi_c^{\mathrm{irr}}(\mathbf{q},\omega)\right]^2 + \left[U_0(\mathbf{q})\mathrm{Im}\chi_c^{\mathrm{irr}}(\mathbf{q},\omega)\right]^2} \tag{88}$$

or, on using Eq. (78),

$$\mathrm{Im}\chi_c(\mathbf{q},\omega) = \frac{q^2}{e^2\omega}\frac{\mathrm{Re}\sigma(\omega)}{\left[1 - \frac{2\pi q}{\omega}\mathrm{Im}\sigma(\mathbf{q},\omega)\right]^2 + \left[\frac{2\pi q}{\omega}\mathrm{Re}\sigma(\mathbf{q},\omega)\right]^2}. \tag{89}$$

To lowest order in *ee* interaction, $\mathrm{Im}\sigma(\mathbf{q},\omega)$ can be replaced by its noninteracting limit: $\mathrm{Im}\sigma(\mathbf{q},\omega) = ne^2/m^*\omega$. Equation (89) is then reduced to

$$\mathrm{Im}\chi_c(\mathbf{q},\omega) = \frac{q^2}{e^2\omega}\frac{\mathrm{Re}\sigma(\mathbf{q},\omega)}{\left[1 - \frac{\omega_{\mathrm{p}}^2(q)}{\omega^2}\right]^2 + \left[\frac{2\pi q}{\omega}\mathrm{Re}\sigma(\mathbf{q},\omega)\right]^2}. \tag{90}$$

The second term in the denominator describes the damping of the plasmon by *ee* interaction. From now and until the end of this section, we will focus on the $T = 0$ limit.

For $v_{\mathrm{D}}q \ll \omega \ll \omega_{\mathrm{p}}(q)$, the unity in the first term and the entire second term in the denominator of Eq. (90) can be neglected, while the conductivity can be approximated by the $O(q^2)$ term in Eq. (86). This yields

$$\mathrm{Im}\chi_c(\mathbf{q},\omega) \approx \frac{q^2\omega^3}{e^2\omega_{\mathrm{p}}^4(q)}\mathrm{Re}\sigma \sim \frac{q^2\omega}{\mu^2}\ln\frac{k_{\mathrm{F}}}{\kappa}. \tag{91}$$

For $\omega_{\mathrm{p}}(q) \ll \omega \ll v_{\mathrm{D}}\kappa$, the leading term in the denominator of Eq. (90) is unity, and the total and irreducible susceptibilities are almost the same:

$$\mathrm{Im}\chi_c(\mathbf{q},\omega) \approx \mathrm{Im}\chi_c^{\mathrm{irr}}(\mathbf{q},\omega) \sim \frac{q^2\omega}{\mu^2}\ln\frac{v_{\mathrm{D}}\kappa}{|\omega|}. \tag{92}$$

As we see, the asymptotics of $\mathrm{Im}\chi_c(\mathbf{q},\omega)$ for $\omega \ll \omega_{\mathrm{p}}(q)$ and $\omega \gg \omega_{\mathrm{p}}(q)$ differ only in the numerical and logarithmic factors. The imaginary part of χ_c, as given by Eq. (85), is plotted in Fig. 7 as a function of frequency at finite q.

We now use the above results to derive the plasmon damping coefficient, deduced from the position of the plasmon pole of Eq. (90) in the complex plane at $\omega = \omega_{\mathrm{p}}(q) - i\Gamma(q)$. According to Eq. (90), the damping coefficient near the plasmon pole is given by

$$\Gamma(q) = \pi q\,\mathrm{Re}\sigma(\mathbf{q},\omega = \omega_{\mathrm{p}}(q)). \tag{93}$$

Substituting Eq. (86) into (93), we obtain

$$\Gamma(q) = \frac{e^2\kappa}{160\pi}\frac{q^2}{k_{\mathrm{F}}^2}\left(\ln\frac{\kappa}{q} + \frac{20}{3}\ln\frac{k_{\mathrm{F}}}{\kappa}\right). \tag{94}$$

It is interesting to compare this result with that for a Galilean-invariant 2D FL with the same number density [59]:

$$\Gamma_{\mathrm{GI}}(q) = \frac{e^4q^2}{12\pi E_{\mathrm{F}}}\ln\frac{k_{\mathrm{F}}}{\kappa}. \tag{95}$$

One can see that the damping coefficients in Eqs. (94) and (95) differ just by the numerical and logarithmic factors. The reason is that the $q = 0$ part of the conductivity in Eq. (86), which is specific for a DFL, and the q^2 part, which is present even in a Galilean-invariant FL, become comparable at $\omega \sim \omega_{\mathrm{p}}(q)$.

VI. OTHER DIRAC SYSTEMS AND RELATION TO THE EXPERIMENT

In this section, we discuss the ω/T scaling of the optical conductivity due to *ee* interactions in other types of DFLs.

A. Bilayer graphene

For the case of Bernal-stacked bilayer graphene (BLG), the effective low-energy Hamiltonian resembles the Dirac-type Hamiltonian of monolayer graphene [Eq. (15b)], but with quadratic in momentum terms on the antidiagonal instead of linear ones [60]. In this approximation, the electron and

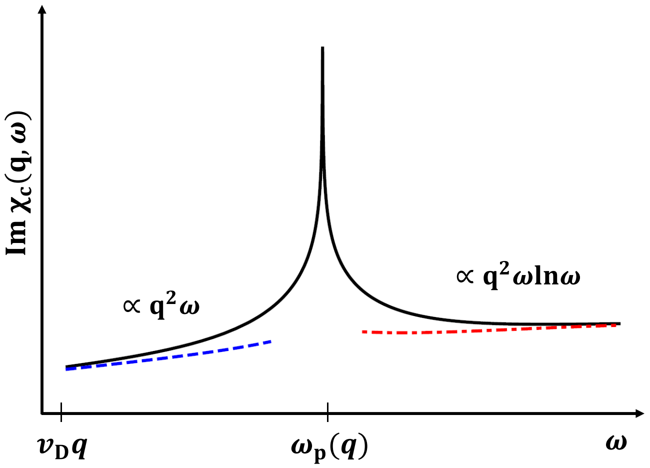

FIG. 7. Log-log scale. Solid: the imaginary part of the total charge susceptibility for doped graphene, as given by Eq. (90) for $q/k_{\mathrm{F}} = 10^{-4}$ and $\alpha_{\mathrm{e}} = e^2/v_{\mathrm{D}} = 0.8$. Dashed and dotted-dashed: the asymptotic limits given by Eq. (91) and Eq. (92), respectively.

hole dispersions are $\epsilon^{\pm}_{\mathbf{k}} = \pm k^2/2\tilde{m}$, where $\tilde{m} = \gamma_1/2v_D^2$ and γ_1 is the coupling between the nearest sites in different layers. Therefore, the system is Galilean invariant, and intraband *ee* scattering does not give rise to a finite optical conductivity. To get a finite conductivity, one needs to account for corrections to the quadratic dispersion. We adopt a standard model for BLG [60], which includes intralayer hopping between A and B sites (with coupling γ_0), interlayer hopping between the nearest A sites and the nearest B sites (with couplings γ_1 and γ_3, respectively), but neglects interlayer hopping between A and B sites.

The BLG spectrum is characterized by two energy scales: γ_1 and $\tilde{m}v_3^2 \sim \gamma_1\gamma_3^2/\gamma_0^2$, where $v_3 = 3\gamma_3 a/2$ and γ_0 is the coupling for in-plane A-B hopping. For a real material, $\gamma_1 \sim \gamma_3 \ll \gamma_0$ (Ref. [60]) and, therefore, $\tilde{m}v_3^2 \ll \gamma_1$. If $\mu \gg \gamma_1$ or $\mu \ll \tilde{m}v_3^2$, the BLG spectrum is essentially a Dirac one with velocities v_D and v_3, respectively. The optical response of BLG in these two regimes is the same as of MLG, and the conductivity is given by Eq. (45), with v_D being replaced by v_3 for $\mu \ll \tilde{m}v_3^2$. A regime specific for BLG occurs for the intermediate range of μ, i.e., $\tilde{m}v_3^2 \ll \mu \ll \gamma_1$. In the case, the conductivity is given by (see Appendix E for details)

$$\mathrm{Re}\sigma_{\mathrm{BLG}}(\omega, T) = e^2\left[c_1\mathcal{D}\left(\frac{T}{\omega}\right)\left(\frac{\omega}{\gamma_1}\right)^2 \ln\frac{v_F\kappa}{|\omega|} + c_2\alpha_e'^2|\ln\alpha_e'|\frac{\tilde{m}v_3^2}{\mu}\mathcal{G}\left(\frac{T}{\omega}\right)\right], \quad (96)$$

where $\mathcal{D}(x) = (1 + 4\pi^2x^2)(3 + 8\pi^2x^2)$ and $\mathcal{G}(x) = 1 + 4\pi^2x^2$ are the DFL and Gurzhi scaling functions, respectively, $v_D = k_F/\tilde{m}$, and $\alpha_e' = e^2/v_D$ is the Coulomb coupling constant for BLG, and $c_{1,2} \sim 1$ are numerical coefficients.

Comparing Eq. (96) with (45), we see that the conductivities of BLG and MLG have similar structure. In both cases, the first terms are due to nonparabolicity of electron spectrum while the second ones are due to scattering between trigonally warped valleys. The difference is in that the energy scale normalizing the frequency in the first term is μ for MLG while it is γ_1 in BLG, and also in that the coefficients of the second terms are different.

B. Surface state of a three-dimensional topological insulator

Another 2D Dirac system is the surface state of a 3D topological insulator, which contains a single Dirac cone at the Γ point of a 2D Brillouin zone. With hexagonal warping taken into account, the dispersion is given by [61]

$$\epsilon^{\pm}_{\mathbf{k}} = \pm\sqrt{v_D^2k^2 + \lambda_{\mathrm{HW}}^2k^2\cos^2(3\theta_{\mathbf{k}})}. \quad (97)$$

If hexagonal warping is neglected, the system is identical to a single-valley version of monolayer graphene. Consequently, the optical conductivity of the surface state is given by Eq. (45) divided by a factor of 2. However, the effect of crystalline anisotropy is different in the two systems. Trigonal warping in graphene, however weak, breaks degeneracy the K and K' valleys. Consequently, intervalley scattering gives rise to a FL behavior of the conductivity, described by the second term in Eq. (52). On the other hand, the Fermi contour of the topological surface state remains convex for μ less than some critical value, which depends on the hexagonal warping parameter λ_{HW}. As long as the Fermi contour is convex, the leading term in the optical conductivity scales as $\max\{\omega^4, T^4\}$ (Ref. [62]), and the dc resistivity exhibits a nonmonotonic T dependence shown in Fig. 4. For μ larger than a critical value, the system exhibits a conventional FL behavior, with $\mathrm{Re}\sigma(\omega, T) \propto \max\{\omega^2, T^2\}$, etc. Except for a narrow range of μ near the convex-to-concave transition [62], the surface state does not exhibit a competition between the DFL and conventional FL behaviors but rather behaves either as a DFL (below the transition) or as a conventional FL (above the transition).

C. Doped three-dimensional Dirac/Weyl metal

Another important class of Dirac-Fermi liquids are 3D Dirac and Weyl metals, doped away from the Dirac point. The properties of these systems are discussed in a number of excellent reviews [15–17,63], so we will limit our discussion to a minimum. In the simplest case, a 3D Dirac/Weyl metal can be described by a system of N_v equivalent Dirac cones with spin degeneracy N_s. For noninteracting electrons and at $T = 0$, the optical conductivity of a Dirac/Weyl metal is given by [64]

$$\mathrm{Re}\sigma(\omega) = \frac{ge^2}{24\pi}\frac{\omega}{v_D}\theta(\omega - 2\mu), \quad (98)$$

where $g = N_sN_v$. As in the 2D case, absorption is possible only due to interband transitions, which are allowed for $\omega > 2\mu$. Equation (98) also describes the limiting case of an undoped system at $\mu = 0$. The linear or quasilinear scaling of $\mathrm{Re}\sigma(\omega)$ with ω for $\omega > 2\mu$ was observed in a number of materials, including HgCdTe [65], $ZrTe_5$ [66], $Eu_2Ir_2O_7$ [67,68], and Cd_3As_2 [69].

As for the case of graphene and other 2D Dirac systems, intraband absorption in doped 3D Weyl/Dirac metals becomes possible for $\omega \ll \mu$ once one takes intraband interaction into account. As long as a Dirac/Weyl metal can be described by a system of N_v equivalent Dirac cones with spin degeneracy N_s, its optical conductivity can be derived along the same lines as for (monolayer) graphene. Skipping the computational details, we present here the final result for the intraband conductivity of a 3D system with an isotropic Dirac spectrum:

$$\mathrm{Re}\sigma(\omega, T) = \frac{Cg^2e^3k_F}{\sqrt{v_D}}\frac{\omega^2}{\mu^2}\left(1 + \frac{4\pi^2T^2}{\omega^2}\right)\left(3 + \frac{8\pi^2T^2}{\omega^2}\right), \quad (99)$$

where $C = 1/3840\pi^2$. In contrast to the 2D case, the integral over the momentum transfers in 3D is not logarithmically divergent, and typical Q are on the order of the interaction radius (κ). Therefore, Eq. (99) is valid only for a long-range interaction, when $\kappa \ll k_F$, rather than for any interaction, as it is the case for 2D. Once this condition is satisfied, the scaling form in Eq. (99) is also valid for any nonparabolic but isotropic dispersion, rather than only for the Dirac one.

D. Relation to the experiment

In this section, we discuss the feasibility of observing our predictions for the *ee* contribution to the conductivity in the

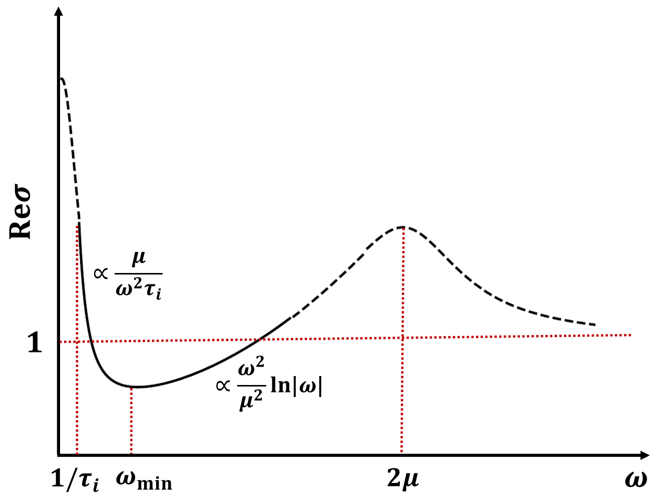

FIG. 8. The conductivity (in units of $e^2/4$) of doped monolayer graphene with impurities for $T = 0$. The solid part of the curve is the result calculated in this paper [Eq. (100)] and the dashed parts are the interpolations between the known limits. $\omega_{\min}$ is given by Eq. (102).

experiment, focusing on the case of monolayer graphene. As it also the case for other materials, the main difficulty with identifying the intraband contribution to the resistivity are the competing effects of scattering by various imperfections (impurities, defects, sample boundaries, etc.) and electron-phonon (*eph*) scattering.

1. Optical measurement

At low temperatures, the main competing mechanism is scattering by imperfections (*ei*). At $T \to 0$ and high enough frequencies, the conductivity assumes a Drude-type form

$$\mathrm{Re}\sigma(\omega) = \frac{ne^2}{m^*\omega^2}\left(\frac{1}{\tau_i} + \frac{1}{\tau_J(\omega,0)}\right), \tag{100}$$

where

$$\frac{1}{\tau_J(\omega,0)} = \frac{1}{80\pi}\frac{\omega^4}{\mu^3}\ln\frac{v_D\kappa}{|\omega|} \tag{101}$$

is obtained by setting $T = 0$ in Eq. (52) and neglecting the trigonal-warping term. For a rough estimate, one can also replace $v_D\kappa$ by μ in the argument of the logarithm. As the frequency increases, the conductivity first decreases as $1/\omega^2$ due the Drude tail of the *ei* contribution, reaches a minimum, and then increases as ω^2 due the second, DFL term in Eq. (100). This behavior is shown in Fig. 8. Neglecting the slowly varying logarithmic factor, the minimum occurs at

$$\omega_{\min} = \mu\left(\frac{160\pi}{g_{dc}}\right)^{1/4}, \tag{102}$$

where $g_{dc} = 2\mu\tau_i$ is the residual conductance of a graphene monolayer at $T = 0$ in units of $e^2/2\pi$. Because our theory is valid only for $\omega \ll \mu$, the DFL increase in the conductivity is seen if $\omega_{\min} \ll \mu$ or $(g_{dc}/160\pi)^{1/4} \gtrsim 1$. Formally, this condition requires $g_{dc} \gg 1$ but, because of a large numerical factor, $160\pi \approx 500$, and also of a small exponent, $\frac{1}{4}$, the condition is quite restrictive, and can only be satisfied in a sample with both high mobility *and* high carrier number density. These conditions are *not* met in the samples used in prior optical measurements [27,28,30]. For example, the highest conductance a sample used in Ref. [27] is $g_{dc} = 160$, at the gate voltage of 71 V, whereas we need g_{dc} to exceed at least 500. This explains why no minima in $\mathrm{Re}\sigma(\omega)$ well below μ were observed in these studies. On the other hand, much higher number densities and thus higher conductances can be achieved in samples with electrolytic gating. For example, the lowest residual resistance of $\rho \approx 38\,\Omega$ measured in Ref. [70] at $n = 1.8 \times 10^{14}$ cm^{-2} corresponds to $g_{dc} \approx 663$, which is above the required value.

If the temperature is not very low, one also needs to worry about the competing effect of *eph* scattering. If flexural phonons in graphene are quenched by a substrate and $\max\{\omega, T\}$ is less than the in-plane optical phonon frequency ($\omega_{\mathrm{opt}} \approx 180$ meV [71,72]), the main mechanism that competes with intraband scattering is scattering by in-plane acoustic phonons. Scattering by acoustic phonons is characterized by the Bloch-Grüneisen temperature ($T_{\mathrm{BG}} = 2k_{\mathrm{F}}v_{\mathrm{s}}$, where v_{s} is the sound velocity), which separates the regimes of inelastic and quasielastic scattering. In the quasielastic regime ($\omega > T_{\mathrm{BG}}$), the *eph* scattering rate is independent of ω, while the *ee* rate continues to increase with ω. This allows one to identify the *ee* contribution, as it was done in classical experiments on optical absorption in good metals [73,74]. When applying the same recipe to graphene, though, one needs to keep in mind that it is a 2D, low-carrier system which harbors a Dirac rather than conventional FL. Because of these features, not only *ee* scattering but also *eph* scattering in graphene are quite distinct from those in good metals. In 2D, the *eph* current relaxation rate scales as T^4 in the inelastic regime and at $\omega = 0$ [70,75]. Extending this result to finite ω, we obtain

$$\frac{1}{\tau_{eph}(\omega,T)} \sim \gamma\frac{(\omega^2 + 4\pi^2T^2)(3\omega^2 + 8\pi^2T^2)}{T_{\mathrm{BG}}^3}, \tag{103}$$

where γ is the dimensionless *eph* coupling constant. In the quasielastic regime, $1/\tau_{eph}(\omega,T) \sim \gamma\max\{T, T_{\mathrm{BG}}\}$ and is independent of ω. For numerical reasons, the actual crossover between the inelastic and quasielastic regimes occurs at $T_{\mathrm{CBG}} \approx 0.2T_{\mathrm{BG}}$ rather at than at T_{BG} itself [70,75]. The asymptotic limits of $1/\tau_{eph}(\omega,T)$ in the different regions of the (ω,T) plane are shown in Fig. 9. At the same time, the electron-electron contribution scales as $\max\{\omega^4\ln|\omega|, T^4\ln T\}$ all the way up to the chemical potential, which is larger than T_{BG} by a factor of at least $v_D/v_s \sim 50$. Even at a rather high number density of 10^{13} cm^{-2}, this interval is very wide: from 25 to 1500 cm^{-1}.

2. dc measurement

In this section, we analyze the feasibility of detecting the intraband contribution in a dc measurement. As shown in Sec. IV C, the T dependence of the current relaxation rate due to a combined effect of the *ei* and interband mechanisms can be described by the following relation:

$$\frac{1}{\tau_J(T)} = \frac{1}{\tau_{\mathrm{i}}}f\left(\frac{\tau_i}{\tau_{ee}^*(T)}\right), \tag{104}$$

where $\tau_{ee}^*(T)$ is given by Eq. (57), and function $f(x)$ is such that $f(x \to 0) = 1 + x + \cdots$, $f(x \to \infty) = 1 - O(1/x)$, and

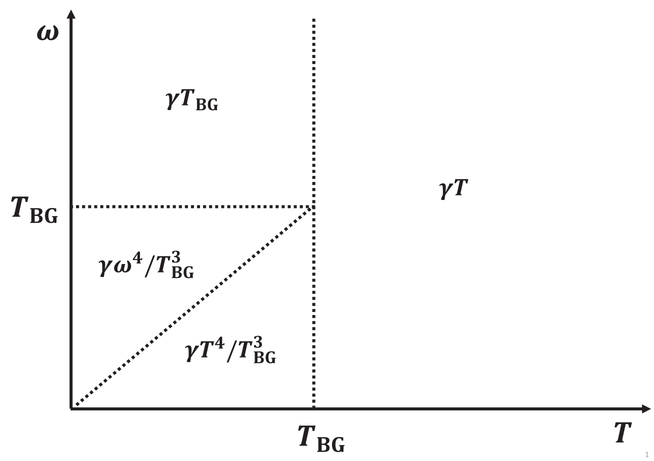

FIG. 9. Frequency and temperature dependencies of the current relaxation rate $1/\tau_{eph}$ for scattering by 2D acoustical phonons in graphene. Here, $T_{\rm BG} = 2k_{\rm F}v_s$ is the Bloch-Grüneisen temperature, v_s is the speed of sound, and γ is the dimensionless coupling constant. Equations in the plot show the asymptotic behavior of $1/\tau_{eph}$ is a given region of ω and T.

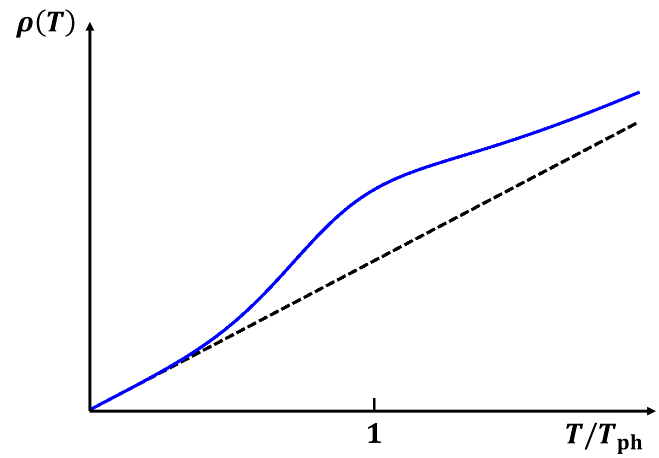

FIG. 10. A sketch of the temperature dependence of the dc resistivity (in a.u.) of doped graphene in the presence of quasielastic electron-phonon scattering and electron-electron scattering. The temperature is normalized to crossover temperature T_{ph}, defined by Eq. (107). The straight dashed line is a pure electron-phonon contribution with a slope deduced from the experiment [70].

$f(x)$ has a maximum at $x \sim 1$ (see Fig. 4). For residual mobility of 10^5 cm^2/Vs and number density $n = 10^{12}$ cm^{-2}, we find $1/\tau_i \approx 0.6$ meV, and thus a crossover temperature at which $\tau_i = \tau_{ee}(T_{\rm i})$ is about 180 K.

The *eph* scattering rate can be written as [70,75]

$$\frac{1}{\tau_{eph}} = \begin{cases} 64\pi^3\gamma T^4/15T_{\rm BG}^3 & \text{for } T \ll T_{\rm BG}, \\ \gamma T & \text{for } T \gg T_{\rm BG}, \end{cases} \tag{105}$$

where $\gamma = D^2\mu/4\rho_{\rm m}v_s^2v_{\rm D}^2 \equiv \mu/\mu_{eph}$, D is the deformation-potential constant, and ρ_m is the mass density of graphene. For $T \gg T_{\rm BG}$ scattering is quasielastic and isotropic; therefore, the scattering rate is proportional to the electronic density of states, which is small at low doping. This smallness is reflected in the large value of parameter μ_{eph}: from the experimentally measured slope of the linear-in-T resistivity [70] we deduce $\mu_{eph} \approx 2.7$ eV; therefore, $\gamma \ll 1$ for all experimentally achievable doping levels.

Coming back to intraband scattering, we estimated a crossover temperature between the two regimes described by Eq. (104) to be around 180 K, which is substantially higher than the Bloch-Grüneisen crossover temperature: $T_{\rm CBG} \sim$ 5–15 K for $n = 10^{12}$–10^{13} cm^{-2}. Therefore, for $T < T_{\rm CBG}$, the electron-electron contribution to the scattering rate is given just by Eq. (52). Up to a logarithm, both the intraband scattering rate and the low-T part of the *eph* scattering rate scale as T^4; however, the former is inversely proportional to μ^3 while the latter is inversely proportional to $T_{\rm BG}^3 \ll \mu^3$. As a result, *eph* scattering dominates over interband one with a large margin: $\tau_{eph}/\tau_{ee}^* \sim 10^{-4}$ at $n = 10^{12}$ cm^{-2}.

For $T > T_{\rm CBG}$ the competition between intraband and *eph* scattering mechanisms is more interesting. In this regime, *eph* scattering is quasielastic and thus plays the same role as *ei* scattering. At sufficiently high T, *eph* scattering is stronger than *ei* one, and one can replace $\tau_{\rm i}$ in Eq. (104) by the high-T limit of Eq. (105); then

$$\frac{1}{\tau_J(T)} = \frac{1}{\tau_{eph}(T)} f\left(\frac{\tau_{eph}(T)}{\tau_{ee}^*(T)}\right). \tag{106}$$

Using Eq. (57) and the first line of Eq. (105), we estimate the crossover temperature between the two regimes described by Eq. (106) as

$$T_{ph} = (15/2\pi^3)^{1/3}\mu^{4/3}/\mu_{eph}^{1/3}, \tag{107}$$

which amounts to $T_{ph} = 270$–1300 K for $n = 10^{12}$–10^{13} cm^{-2}. For $T < T_{ph}$, the resistivity varies faster than T, i.e., as $T + \text{const} \times T^4 \ln T$, goes over a hump at $T \sim T_{ph}$, and then approaches the linear T dependence again for $T > T_{ph}$ (see Fig. 10).

On the experimental side, the resistivity of graphene at low doping exhibits a crossover from a linear-T dependence below 200 K to a superlinear one above 200 K [76,77], while no such a crossover is observed at higher doping [70]. This is consistent with the behavior predicted by Eq. (107) because the crossover temperature increases with n as $T_{ph} \propto n^{2/3}$. For the lowest n in Ref. [70] ($n = 1.36 \times 10^{13}$ cm^{-2}) we find $T_{ph} \approx 1550$ K, which is well above the highest temperature measured. On the other hand, T_{ph} is within the measurement range for lower n used in Refs. [76,77]. A superlinear resistivity was attributed alternatively to two-phonon scattering by flexural phonons [76,78], scattering on surface phonons in the SiO_2 substrate [77,79], or else to a crossover between degenerate and nondegenerate regimes in electron scattering by charged impurities [80]. We submit, however, that intraband scattering may also provide a plausible explanation of the superlinear scaling.

VII. CONCLUSIONS

In this paper, we have studied the effect of intraband electron-electron (*ee*) interaction on the optical conductivity of a non-Galilean-invariant but isotropic Fermi liquid (FL), focusing primarily on one representative example: a 2D Dirac-Fermi liquid (DFL). We studied a model of doped monolayer graphene with two nondegenerate valleys at $K_\pm$ points and considered both intravalley and intervalley scattering. If trigonal warping of Fermi contours is neglected, the valleys become degenerate. We showed that the leading contribution to the optical conductivity comes from processes with small momentum transfers $Q \ll k_F$. In this case, the intravalley and intervalley interactions contribute equally, and the current relaxation rate acquires a universal form, reproduced below for the reader's convenience:

$$1/\tau_J \propto (\omega^2 + 4\pi^2 T^2)(3\omega^2 + 8\pi^2 T^2) \ln \frac{\Lambda}{\max\{|\omega|, T\}}. \quad (108)$$

This form replaces the universal Gurzhi form for a conventional FL, Eq. (1). In 2D, Eq. (108) form is *universal*: it is valid for any form of interaction (as long as it is finite at $Q \to 0$ and vanishes at $Q \to \infty$) and for any isotropic but nonparabolic dispersion, rather than only for a Dirac one. The quartic (as opposed to quadratic) scaling reflects the fact that the interaction between electrons on an isotropic Fermi surface (FS) does not relax the current, and one needs to invoke the states close to but away from the FS.

Weak anisotropy due to trigonal warping breaks the valley degeneracy and, as result, intervalley scattering gives rise to a Gurzhi-type contribution to the current relaxation rate. Although this contribution scales as $\max\{\omega^2, T^2\}$, it comes with a small prefactor proportional to doping, and thus competes with a quartic, DFL contribution.

Equation (108) is valid only for $\omega \gg 1/\tau_J(0, T)$ and *cannot* be extended to the static limit. In the absence of other current-relaxing processes, $1/\tau_J(\omega \to 0, T)$ is given by the sum of delta function, peaked at $\omega = 0$, and a regular part in Eq. (108), evaluated at $\omega = 0$. Such a form is characteristic for any non-Galilean-invariant system, which has finite optical conductivity due to *ee* interactions at finite frequency but infinite dc conductivity.

We also studied the interplay between electron-impurity (*ei*) and electron-electron scattering via a semiclassical Boltzmann equation. If *ee* scattering is less frequent than *ei* one, the Mathiessen rule is satisfied, in a sense that the total current relaxation rate is the sum of the *ei* rate and the quartic correction due to *ee* interaction.

In the opposite limit of more frequent *ee* scattering, the optical conductivity can be written as the sum of two Drude peaks, with widths given by the *ei* and *ee* relaxation rates, respectively. This last result can also be extended to the dc limit, where the resistivity approaches the residual value for temperatures both below and *above* a crossover temperature T_i, at which the *ei* and inter-band current relaxation rates are equal. In-between the two limits, the resistivity varies nonmonotonically with T, exhibiting a maximum at $T \sim T_i$ (see Fig. 4).

We also have studied the dynamical charge response of doped graphene, at $T = 0$ and in the absence of disorder, to one-loop order in a dynamically screened Coulomb interaction. We showed the imaginary part of the (irreducible) charge susceptibility scales as $\mathrm{Im}\chi_c^{\mathrm{irr}}(\mathbf{q}, \omega) \propto q^2\omega \ln|\omega|$ or q^4/ω^3, for ω below and above the plasmon frequency at given q. The q^2 term in $\mathrm{Im}\chi_c^{\mathrm{irr}}(\mathbf{q}, \omega)$ reproduces the result for $\mathrm{Re}\sigma(\omega, T = 0)$ via the Einstein relation.

Towards the end, we discussed the optical conductivity for a number of related systems: bilayer graphene, the surface state of a 3D topological insulator, 3D Dirac/Weyl metals, as well as the implications of our results for the existing and future experiments. The predicted $\omega^2 \ln|\omega|$ scaling of the conductivity has the best chance to be observed in monolayer graphene with very high residual conductivity, $\gtrsim 600\, e^2/h$, which requires samples with both high mobility *and* high carrier number density.

ACKNOWLEDGMENTS

We are grateful to D. Bandurin, A. Chubukov, L. Glazman, A. Goyal, J. Hamlin, P. Hirschfeld, A. Kumar, A. Levchenko, A. Rosch, J. Schmalian, O. Vafek, G. Vignale, and V. Yudson for stimulating discussions. This work was supported by the National Science Foundation under Grant No. NSF DMR-1720816 (P.S. and D.L.M.) and, in part, under Grant No. NSF PHY-1748958, administered via Kavli Institute for Theoretical Physics, Santa Barbara, California (D.L.M.). A.P. acknowledges support from the European Commission under the EU Horizon 2020 MSCA-RISE-2019 program (project 873028 HYDROTRONICS), and from the Leverhulme Trust under the Grant No. RPG-2019-363.

APPENDIX A: OPTICAL CONDUCTIVITY AT FINITE T AND ω FROM THE KUBO FORMULA

In this Appendix, we derive a general expression for the optical conductivity at finite temperature and frequency, to lowest order in electron-electron interaction, Eq. (32) of the main text. We extend the formalism developed by Rosch [8] finite temperatures. The Kubo formula reads as

$$\sigma_{\ell m}(\mathbf{q}, \omega) = \frac{i}{\omega}\left[\Pi_{\ell m}(\mathbf{q}, \omega) + \Pi^{\mathrm{dia}}_{\ell m}\right], \quad (A1)$$

where $\ell, m \in \{x, y\}$,

$$\Pi_{\ell m}(\mathbf{q}, \omega) = -i \int_{-\infty}^{\infty} dt\, e^{i\omega(t-t')}\Theta(t-t')\langle[J_\ell^\dagger(\mathbf{q}, t), J_m(\mathbf{q}, t')]\rangle$$
$$= -i \int_0^{\infty} dt\, e^{i\omega t}\langle[J_\ell^\dagger(\mathbf{q}, t), J_m(\mathbf{q}, 0)]\rangle \quad (A2)$$

is the current-current correlation function, and angular brackets denote quantum-mechanical and thermal averaging [81]. Next, $\Pi^{\mathrm{dia}}_{\ell m}$ is the diamagnetic part of the conductivity. Because gauge invariance guarantees that $\Pi^{\mathrm{dia}}_{\ell m} = -\Pi_{\ell m}(\mathbf{q} = 0, \omega \to 0)$ (Ref. [48]), an explicit form of $\Pi^{\mathrm{dia}}_{\ell m}$ is not needed.

For a homogeneous time-dependent electric field, $\mathbf{q} = 0$ and $\Pi_{\ell m}(\omega) \equiv \Pi_{\ell m}(0, \omega)$ becomes

$$\Pi_{\ell m}(\omega) = -i \int_0^{\infty} dt\, e^{i\omega t}\langle[J_\ell(t), J_m(0)]\rangle. \quad (A3)$$

Integrating by parts and using the Heisenberg equation of motion $d\mathbf{J}/dt = -i[\mathbf{J}(t), H]$ along with the cyclic property of a trace, we rewrite $\Pi_{\ell m}(\omega)$ as

$$\Pi_{\ell m}(\omega) = \frac{1}{i\omega}\langle[J_\ell(0), J_m(0)]\rangle - \int_0^\infty dt\,\frac{e^{i\omega t}}{\omega}\left\langle\left[\frac{dJ_\ell(t)}{dt}, J_m(0)\right]\right\rangle$$
$$= \frac{i}{\omega}\int_0^\infty dt\, e^{i\omega t}\langle[J_\ell(t), [J_m(0), H]]\rangle, \quad \text{(A4)}$$

where H is the total Hamiltonian. One more integration by parts leads to

$$\omega^2\Pi_{\ell m}(\omega) = -\langle[J_\ell(0), K_m(0)]\rangle - \langle[K_\ell(t), K_m(0)]\rangle_\omega, \quad \text{(A5)}$$

where $\mathbf{K}(t) = [\mathbf{J}(t), H]$ and $\langle K_\ell(t), K_m(0)\rangle_\omega = -i\int_0^\infty dt\, e^{i\omega t}\langle[[J_\ell(t), H], [J_m(0), H]]\rangle$. Because the first term in the equation above is purely real, the real part of the optical conductivity is given by

$$\text{Re}\sigma_{\ell m}(\omega, T) = \frac{1}{\omega^3}\text{Im}\langle[K_\ell(t), K_m(0)]\rangle_\omega. \quad \text{(A6)}$$

For a long-range interaction, the Hamiltonian projected onto the conduction band is given by

$$H = \sum_{\varsigma\mathbf{k}s}\epsilon_{\varsigma,\mathbf{k},s}\alpha^\dagger_{\varsigma,\mathbf{k},s}\alpha_{\varsigma,\mathbf{k},s} + \frac{1}{2}\sum_{\varsigma\varsigma'}\sum_{\mathbf{kpk'p'}}\sum_{ss'}U_0(|\mathbf{k}-\mathbf{k}'|)$$
$$\times\,\alpha^\dagger_{\varsigma,\mathbf{k}',s}\alpha^\dagger_{\varsigma',\mathbf{p}',s'}\alpha_{\varsigma',\mathbf{p},s'}\alpha_{\varsigma,\mathbf{k},s}\delta(\mathbf{k}'+\mathbf{p}'-\mathbf{k}-\mathbf{p}), \quad \text{(A7)}$$

where ς is the valley index. For the case of graphene, $\varsigma = \pm$ denote the two Dirac points K_ς. Because the interaction part of H is of density-density type, it commutes with the charge-density operator at $\mathbf{q} = 0$, and the total current is obtained by commuting the charge-density operator with the free part of H:

$$\mathbf{J} = e\sum_{\varsigma\mathbf{k}s}\mathbf{v}_{\varsigma,\mathbf{k}}\alpha^\dagger_{\varsigma,\mathbf{k},s}\alpha_{\varsigma,\mathbf{k},s}, \quad \text{(A8)}$$

where $\mathbf{v}_{\varsigma,\mathbf{k}} = \nabla_\mathbf{k}\epsilon_{\varsigma,\mathbf{k},s}$ is the group velocity. Correspondingly, $\mathbf{K}(t)$ is given by

$$\mathbf{K}(t) = [\mathbf{J}(t), H] = \frac{e}{2}\sum_{\varsigma\varsigma'}\sum_{\mathbf{kpk'p'}}\sum_{ss'}U_0(|\mathbf{k}-\mathbf{k}'|)(\mathbf{v}_{\varsigma,\mathbf{k}'}+\mathbf{v}_{\varsigma',\mathbf{p}'}-\mathbf{v}_{\varsigma,\mathbf{k}}-\mathbf{v}_{\varsigma',\mathbf{p}})\alpha^\dagger_{\varsigma,\mathbf{k}',s}\alpha^\dagger_{\varsigma',\mathbf{p}',s'}\alpha_{\varsigma',\mathbf{p},s'}\alpha_{\varsigma,\mathbf{k},s}\delta(\mathbf{k}'+\mathbf{p}'-\mathbf{k}-\mathbf{p}), \quad \text{(A9)}$$

and its correlator by

$$\langle[K_\ell(t), K_m(0)]\rangle_\omega = -i\frac{e^2}{4}\int_0^\infty dt\, e^{i\omega t}\sum_{\varsigma_1\varsigma_1'\varsigma_2\varsigma_2'}\sum_{s_1s_1's_2s_2'}\sum_{\mathbf{k}_1\mathbf{p}_1\mathbf{k}_1'\mathbf{p}_1'}\sum_{\mathbf{k}_2\mathbf{p}_2\mathbf{k}_2'\mathbf{p}_2'}$$
$$\times\left(v^\ell_{\varsigma_1,\mathbf{k}_1'}+v^\ell_{\varsigma_1',\mathbf{p}_1'}-v^\ell_{\varsigma_1,\mathbf{k}_1}-v^\ell_{\varsigma_1',\mathbf{p}_1}\right)\left(v^m_{\varsigma_2,\mathbf{k}_2'}+v^m_{\varsigma_2',\mathbf{p}_2'}-v^m_{\varsigma_2,\mathbf{k}_2}-v^m_{\varsigma_2',\mathbf{p}_2}\right)$$
$$\times\,U_0(|\mathbf{k}_1-\mathbf{k}_1'|)U_0(|\mathbf{k}_2-\mathbf{k}_2'|)\delta(\mathbf{k}_1'+\mathbf{p}_1'-\mathbf{k}_1-\mathbf{p}_1)\delta(\mathbf{k}_2'+\mathbf{p}_2'-\mathbf{k}_2-\mathbf{p}_2)$$
$$\times\left\langle\left[\alpha^\dagger_{\varsigma_1,\mathbf{k}_1',s_1}(t)\alpha^\dagger_{\varsigma_1',\mathbf{p}_1',s_1'}(t)\alpha_{\varsigma_1',\mathbf{p}_1,s_1'}(t)\alpha_{\varsigma_1,\mathbf{k}_1,s_1}(t), \alpha^\dagger_{\varsigma_2,\mathbf{k}_2',\varsigma_2}(0)\alpha^\dagger_{\varsigma_2',\mathbf{p}_2',\varsigma_2'}(0)\alpha_{\varsigma_2',\mathbf{p},s_2'}(0)\alpha_{\gamma,\mathbf{k}_2,\varsigma_2}(0)\right]\right\rangle. \quad \text{(A10)}$$

Since $\langle[K_\ell(t), K_m(0)]\rangle_\omega$ is already quadratic in the interaction, to lowest order the expectation value of the commutator above can be calculated for free fermions. Using the time dependence of the operators, $\alpha_{\varsigma,\mathbf{k},s}(t) = \alpha_{\varsigma,\mathbf{k},s}e^{-i\epsilon_{\varsigma,\mathbf{k}}t}$, the integration over time is readily carried out.

Applying Wick's theorem and using that $\langle\alpha^\dagger_{\varsigma,\mathbf{k},s}\alpha_{\varsigma,\mathbf{k},s}\rangle$ gives the Fermi function $n_\text{F}(\epsilon_{\varsigma,\mathbf{k}})$, we obtain the real part of the conductivity as

$$\text{Re}\sigma_{\ell m}(\omega, T) = \frac{2\pi e^2(1-e^{-\beta\omega})}{\omega^3}\sum_{\varsigma\varsigma'}\sum_{\mathbf{kpk'p'}}\left(v^\ell_{\varsigma,\mathbf{k}'}+v^\ell_{\varsigma',\mathbf{p}'}-v^\ell_{\varsigma,\mathbf{k}}-v^\ell_{\varsigma',\mathbf{p}}\right)\left(v^m_{\varsigma,\mathbf{k}'}+v^m_{\varsigma',\mathbf{p}'}-v^m_{\varsigma,\mathbf{k}}-v^m_{\varsigma',\mathbf{p}}\right)$$
$$\times\,U_0(|\mathbf{k}-\mathbf{k}'|)\left[U_0(|\mathbf{k}-\mathbf{k}'|)-\delta_{\varsigma\varsigma'}\delta_{\varsigma\varsigma'}\frac{U_0(|\mathbf{p}-\mathbf{k}'|)}{2}\right]$$
$$\times\,n_\text{F}(\epsilon_{\varsigma,\mathbf{k}'})n_\text{F}(\epsilon_{\varsigma',\mathbf{p}'})[1-n_\text{F}(\epsilon_{\varsigma,\mathbf{k}})][1-n_\text{F}(\epsilon_{\varsigma',\mathbf{p}})]\delta(\omega+\epsilon_{\varsigma',\mathbf{p}'}+\epsilon_{\varsigma,\mathbf{k}'}-\epsilon_{\varsigma,\mathbf{k}}-\epsilon_{\varsigma',\mathbf{p}})\delta(\mathbf{k}'+\mathbf{p}'-\mathbf{k}-\mathbf{p}). \quad \text{(A11)}$$

If the crystal symmetry is such that $\sigma_{xx} = \sigma_{yy} = \sigma_{zz} \equiv \sigma$, while $\sigma_{\ell\neq m} = 0$, the last formula is reduced to Eq. (32) of the main text.

APPENDIX B: INTEGRAL OVER ENERGIES

The triple integral over energies in Eq. (43) is given by

$$I = \int d\epsilon_\mathbf{k}\int d\epsilon_\mathbf{p}\int d\Omega[(2\Omega+\omega)^2+\omega^2]n_\text{F}(\epsilon_\mathbf{k}+\Omega)n_\text{F}(\epsilon_\mathbf{p}-\omega-\Omega)[1-n_\text{F}(\epsilon_\mathbf{k})][1-n_\text{F}(\epsilon_\mathbf{p})]. \quad \text{(B1)}$$

Introducing dimensionless variables $x = \epsilon_\mathbf{k}/T$, $y = \epsilon_\mathbf{p}/T$, $z = \Omega/T$, and $a = \omega/T$, we obtain

$$I = T^5\int_{-\infty}^\infty dx\int_{-\infty}^\infty dy\int_{-\infty}^\infty dz[(2z+a)^2+a^2]\frac{e^x}{e^x+1}\frac{e^y}{e^y+1}\frac{1}{e^{z+x}+1}\frac{1}{e^{y-z-a}+1}. \quad \text{(B2)}$$

Substituting $u = e^x$ and $v = e^y$, we get

$$\begin{aligned} I &= T^5 e^a \int_0^\infty du \int_0^\infty dv \int_{-\infty}^\infty dz[(2z+a)^2 + a^2] \frac{1}{u+1} \frac{1}{v+1} \frac{1}{e^{-z}+u} \frac{1}{e^{z+a}+v} \\ &= T^5 e^a \int_0^\infty du \int_0^\infty dv \int_{-\infty}^\infty dz[(2z+a)^2 + a^2] \frac{1}{e^{-z}-1}\left(\frac{1}{u+1} - \frac{1}{e^{-z}+u}\right) \frac{1}{e^{z+a}-1}\left(\frac{1}{v+1} - \frac{1}{e^{z+a}+v}\right). \end{aligned} \tag{B3}$$

Integrals over u and v yield

$$\begin{aligned} I &= -T^5 e^a \int_{-\infty}^\infty dz \frac{z(z+z)[(2z+z)^2 + a^2]}{(e^{-z}-1)(e^{z+a}-1)}, \\ &= T^5 \frac{(3a^5 + 20\pi^2 a^3 + 32\pi^4 a)}{15(1-e^{-a})} = \frac{a(a^2+4\pi^2)(3a^2+8\pi)}{15(1-e^{-a})}, \end{aligned} \tag{B4}$$

which is Eq. (43) of the main text.

APPENDIX C: OPTICAL CONDUCTIVITY FROM INTERVALLEY SCATTERING

In this Appendix, we present the derivation of Eq. (49) for the contribution of intervalley scattering to the optical conductivity. With trigonal warping of the isoenergetic contours taken account according to Eqs. (17a)–(17c), the group velocity in Cartesian coordinates is given by

$$\mathbf{v}_{\varsigma,\mathbf{k}} = \nabla_\mathbf{k} \epsilon_{\varsigma,\mathbf{k}} = \mathbf{v}^\mathrm{D}_\mathbf{k} + \mathbf{v}^\mathrm{TW}_{\varsigma,\mathbf{k}}, \tag{C1}$$

where

$$\begin{aligned} \mathbf{v}^\mathrm{D}_\mathbf{k} &= \frac{v_\mathrm{D}}{k}(k_x\hat{x} + k_y\hat{y}), \\ \mathbf{v}^\mathrm{TW}_{\varsigma,\mathbf{k}} &= \frac{\varsigma v_\mathrm{D} a}{4}\left(\frac{\left(2k_x^4 + 3k_x^2k_y^2 - 3k_y^4\right)}{k^3}\hat{x} - \frac{k_xk_y\left(7k_x^2+3k_y^2\right)}{k^3}\hat{y}\right). \end{aligned} \tag{C2}$$

A change in the velocity due to an *ee* collision can be written as

$$\mathbf{v}_{+,\mathbf{k}-\mathbf{Q}} + \mathbf{v}_{-,\mathbf{p}+\mathbf{Q}} - \mathbf{v}_{+,\mathbf{k}} - \mathbf{v}_{-,\mathbf{p}} = \Delta\mathbf{v}^\mathrm{D} + \Delta\mathbf{v}^\mathrm{TW}, \tag{C3}$$

where $\Delta\mathbf{v}^\mathrm{D}$ and $\Delta\mathbf{v}^\mathrm{TW}$ are contributions from the Dirac and trigonally warped parts of dispersion, respectively. To leading order in $k_\mathrm{F}a \ll 1$, one can take the dispersion to be isotropic everywhere else in Eq. (47) and drop the valley index. Accordingly, the contour integrals are replaced by $\oint d\ell_\mathbf{k}/v_\mathbf{k} = [k_\mathrm{F}/(2\pi v_\mathrm{D})]\int d\theta_{\mathbf{kQ}}$. Next, for electrons on the FS one can drop ω in the δ functions. Then the kinematic constraints on the angles are still the same as for a circular FS, i.e., $\theta_{\mathbf{kQ}} = \pm\pi/2$ and $\theta_{\mathbf{pQ}} = \pm\pi/2$. Finally, for small-angle scattering $\Delta\mathbf{v}$ can be expanded to first order in $\mathbf{Q}$ as

$$\Delta\mathbf{v}^\mathrm{TW} = -(\mathbf{Q}\cdot\nabla_\mathbf{k})\mathbf{v}^\mathrm{TW}_{+,\mathbf{k}} + (\mathbf{Q}\cdot\nabla_\mathbf{p})\mathbf{v}^\mathrm{TW}_{-,\mathbf{p}} = -(\mathbf{Q}\cdot\nabla_\mathbf{k})\mathbf{v}^\mathrm{TW}_{+,\mathbf{k}} - (\mathbf{Q}\cdot\nabla_\mathbf{p})\mathbf{v}^\mathrm{TW}_{+,\mathbf{p}}. \tag{C4}$$

Since an electron pair with opposite velocities carries zero current both before and after the collision, Cooper channel ($\mathbf{p} = -\mathbf{k}$) should not contribute to current relaxation. Indeed, because $\mathbf{v}^\mathrm{TW}_{\varsigma,-\mathbf{k}} = \mathbf{v}^\mathrm{TW}_{\varsigma,\mathbf{k}}$, it follows that $\Delta\mathbf{v}^\mathrm{TW} = 0$ for the Cooper channel, and we need to consider only the collinear channel ($\mathbf{p} = \mathbf{k}$). Using $\theta_\mathbf{k} = \theta_{\mathbf{kQ}} + \theta_\mathbf{Q}$ with $\theta_{\mathbf{kQ}} = \pm\pi/2$, we obtain in polar coordinates

$$\Delta\mathbf{v}^\mathrm{TW} = v_\mathrm{D}(k_\mathrm{F}a)\frac{Q}{k_\mathrm{F}}(3\cos(3\theta_\mathbf{Q})\hat{\mathbf{k}} - 7\sin(3\theta_\mathbf{Q})\hat{\theta}_\mathbf{k}). \tag{C5}$$

Equation (47) is then reduced to

$$\begin{aligned} \mathrm{Re}\sigma^\mathrm{inter}(\omega,T) &= e^2\frac{N_\mathrm{F}^2}{2\pi\omega^3}(1-e^{-\beta\omega})\int\frac{d^2Q}{(2\pi)^2}(\Delta\mathbf{v}^\mathrm{TW})^2U^2(\mathbf{Q})\frac{1}{(v_\mathrm{D}Q)^2} \\ &\times \int d\epsilon_\mathbf{k}\int d\epsilon_\mathbf{p}\int d\Omega\, n_\mathrm{F}(\epsilon_\mathbf{k}+\Omega)n_\mathrm{F}(\epsilon_\mathbf{p}-\Omega-\omega)[1-n_\mathrm{F}(\epsilon_\mathbf{k})][1-n_\mathrm{F}(\epsilon_\mathbf{p})]. \end{aligned} \tag{C6}$$

Averaging $(\Delta\mathbf{v}^\mathrm{TW})^2$ over $\theta_\mathbf{Q}$ yields

$$\int_0^{2\pi}\frac{d\theta_\mathbf{Q}}{2\pi}(\Delta\mathbf{v}^\mathrm{TW})^2 = 29(v_\mathrm{D}Qa)^2. \tag{C7}$$

The integral over Q is solved to leading-logarithm order as

$$\int dQ\, QU^2(\mathbf{Q}) = (2\pi e^2)^2\ln\frac{k_\mathrm{F}}{\kappa}, \tag{C8}$$

while the energy integrals in Eq. (C6) give

$$\int d\epsilon_{\mathbf{k}} \int d\epsilon_{\mathbf{p}} \int d\Omega \quad \times n_{\mathrm{F}}(\epsilon_{\mathbf{k}}+\Omega)n_{\mathrm{F}}(\epsilon_{\mathbf{p}}-\Omega-\omega)[1-n_{\mathrm{F}}(\epsilon_{\mathbf{k}})][1-n_{\mathrm{F}}(\epsilon_{\mathbf{p}})] = \frac{\omega(\omega^2+4\pi^2T^2)}{6(1-e^{-\beta\omega})}. \tag{C9}$$

Collecting everything together, we obtain Eq. (49) of the main text.

APPENDIX D: CHARGE SUSCEPTIBILITY

1. Self-energy and exchange diagram for the irreducible charge susceptibility

In this Appendix, we calculate the sum of diagrams a and b ("self-energy"), and c ("exchange") in Fig. 6 for doped monolayer graphene. For $\omega \ll 2\mu$, interband transitions are neglected and the system is effectively reduced to a single-band one. Also, the matrix elements in the Green functions for doped graphene can be replaced by unities in the forward-scattering limit. Under these approximations, the sum of the three diagrams can be written as [58]

$$\chi_c^{(\mathrm{S,E})}(\mathbf{q},\omega_m) = -\iiint\int \frac{d^2Q\, d^2k\, d\Omega_l d\varepsilon_n}{(2\pi)^{2(D+1)}} U(\mathbf{Q},\Omega_l)\frac{(\epsilon_{\mathbf{k+q}}-\epsilon_{\mathbf{k}}-\epsilon_{\mathbf{k+Q+q}}+\epsilon_{\mathbf{k+Q}})^2}{(i\omega_m-\epsilon_{\mathbf{k+Q+q}}+\epsilon_{\mathbf{k+Q}})^2(i\omega_m-\epsilon_{\mathbf{k+q}}+\epsilon_{\mathbf{k}})^2}$$
$$\times[G(\mathbf{k},\varepsilon_n)-G(\mathbf{k+q},\varepsilon_n+\omega_m)][G(\mathbf{k+Q},\varepsilon_n+\Omega_l)-G(\mathbf{k+Q+q},\varepsilon_n+\Omega_l+\omega_m)]. \tag{D1}$$

We are interested in long-wavelength excitations with momenta $q \ll \omega/v_{\mathrm{D}} \ll k_{\mathrm{F}}$. In this case, the denominators in the fraction in the first line of Eq. (D1) can be replaced by $i\omega_m$. Also, typical momentum transfers are assumed to be much smaller than k_{F}. Therefore, the single-particle dispersion in the numerator of the same fraction can be expanded both in q and Q. For a Dirac dispersion, the leading-order term in this expansion reads as

$$\epsilon_{\mathbf{k+q}}-\epsilon_{\mathbf{k}}-\epsilon_{\mathbf{k+Q+q}}+\epsilon_{\mathbf{k+Q}} \approx -\frac{qQv_{\mathrm{D}}}{k_{\mathrm{F}}}\sin\theta\sin\theta', \tag{D2}$$

where θ and θ' are the angles that $\mathbf{q}$ and $\mathbf{Q}$ make with $\mathbf{k}$, respectively. With these simplifications, Eq. (D1) is reduced to

$$\chi_c^{(\mathrm{S,E})}(\mathbf{q},\omega_m) = -\frac{1}{\omega_m^4k_{\mathrm{F}}^2}\iiint\int \frac{d^2Q\, d^2k\, d\Omega_l d\varepsilon_n}{(2\pi)^6} U(\mathbf{Q},\Omega_l)(qQv_{\mathrm{D}}\sin\theta\ \sin\theta')^2$$
$$\times[G(\mathbf{k},\varepsilon_n)-G(\mathbf{k+q},\varepsilon_n+\omega_m)][G(\mathbf{k+Q},\varepsilon_n+\Omega_l)-G(\mathbf{k+Q+q},\varepsilon_n+\Omega_l+\omega_m)]. \tag{D3}$$

Next, we integrate the products of the Green's functions in the equation above first over ε_n, and then over $\epsilon_{\mathbf{k}}$ and θ, and neglect q compared to Q in the final result. This gives

$$\chi_c^{(\mathrm{S,E})}(\mathbf{q},\omega_m) = -\frac{iN_{\mathrm{F}}q^2v_{\mathrm{D}}^2}{2k_F^2\omega_m^4}\int\frac{Q^3dQ}{2\pi}\int\frac{d\Omega_l}{(2\pi)}U(\mathbf{Q},\Omega_l)$$
$$\times\frac{d\theta'}{2\pi}\sin^2\theta'\left[\frac{2\Omega_l}{i\Omega_l-v_{\mathrm{D}}\hat{\mathbf{k}}\cdot\mathbf{Q}}-\frac{\Omega_l+\omega_m}{i(\Omega_l+\omega_m)-v_{\mathrm{D}}\hat{\mathbf{k}}\cdot\mathbf{Q}}-\frac{\Omega_l-\omega_m}{i(\Omega_l-\omega_m)-v_{\mathrm{D}}\hat{\mathbf{k}}\cdot\mathbf{Q}}\right], \tag{D4}$$

where N_{F} is the density of states. Now we integrate over θ', using

$$\int_0^{2\pi}\frac{dx}{2\pi}\frac{\sin^2x}{iy-\cos x} = i(y-\mathrm{sgn}y\sqrt{y^2+1}), \tag{D5}$$

to get

$$\chi_c^{(\mathrm{S,E})}(\mathbf{q},\omega_m) = -\frac{N_{\mathrm{F}}q^2v_{\mathrm{D}}}{2k_{\mathrm{F}}^2\omega_m^4}\int\frac{Q^3dQ}{2\pi}\int\frac{d\Omega_l}{(2\pi)}U(\mathbf{Q},\Omega_l)\frac{1}{Q^2}\big[2\omega_m^2+2|\Omega_l|\sqrt{\Omega_l^2+(v_{\mathrm{D}}Q)^2}$$
$$-|\Omega_l+\omega_m|\sqrt{(\Omega_l+\omega_m)^2+(v_{\mathrm{D}}Q)^2}-|\Omega_l-\omega_m|\sqrt{(\Omega_l-\omega_m)^2+(v_{\mathrm{D}}Q)^2}\big]. \tag{D6}$$

Now we will simplify the form of the interaction potential. First, we notice that a static interaction cannot give rise to a finite imaginary part of the susceptibility outside the particle-hole continuum. Therefore, we can subtract off a static screened Coulomb potential from the dynamical one in Eq. (D6). Next, we assume first and verify thereafter that typical Q are such that $\Omega \ll v_{\mathrm{D}}Q$. Then the difference of the dynamical and static screened Coulomb potentials can be expanded in $x \equiv \Omega_l \ll v_{\mathrm{D}}Q$ as

$$U_{\mathrm{dyn}}(Q,\Omega_l) = U(Q,\Omega_l)-U(Q,0) = \frac{1}{N_{\mathrm{F}}}a^2x(1+ax+(a^2-1/2)x^2+\cdots), \tag{D7}$$

where $a = \kappa/(Q+\kappa)$. We will see later on that one does need to keep $O(x^3)$ terms in the series above, whereas for a conventional FL it suffices to keep only $O(x)$ terms.

Next we integrate over Ω_l in Eq. (D6) to obtain

$$\int d\Omega_l U_{\rm dyn}(\mathbf{Q},\Omega_l) = \frac{2v_{\rm D}Q}{N_{\rm F}}a^2\int_0^\Lambda dx\, x[1+ax+(a^2-1/2)x^2] \times\left[2y^2+2x\left(1+\frac{x^2}{2}\right)-(x+y)\left(1+\frac{(x+y)^2}{2}\right)-|x-y|\left(1+\frac{(x-y)^2}{2}\right)\right] = -\frac{2}{3}v_{\rm D}Qa^2y^3-\frac{1}{5}v_{\rm D}Qa^4y^5+\mathcal{I}(\Lambda)+O(y^2)+O(y^4)\ldots, \tag{D8}$$

where $y=\omega_m/v_{\rm D}Q>0$ and $\mathcal{I}(\Lambda)$ is some function of the upper cutoff, which is irrelevant in what follows. Terms of the order $O(y^2, y^4\ldots)$ do not contribute to $\mathrm{Im}\,\chi_c$ and are omitted. Finally, the remaining integral over Q reads as

$$\chi_c^{(S,E)}(\mathbf{q},\omega_m) = \frac{e^4}{\pi^2 v_{\rm D}^2}\left[\frac{2}{3}\frac{q^2}{\omega_m}\int_0^{\Lambda_Q}\frac{dQ\,Q}{(Q+\kappa)^2}+\frac{1}{5}\frac{q^2\omega_m\kappa^2}{v_{\rm D}^2}\int_{|\omega_m|/v_{\rm D}}^\infty\frac{dQ}{Q}\frac{1}{(Q+\kappa)^4}\right], \tag{D9}$$

where Λ_Q is some upper cutoff. We will complete the integral over Q after combining Eq. (D9) with a contribution from the AL diagrams. Then it will be seen that the first term in Eq. (D9) cancels out and, therefore, a choice of Λ_Q is irrelevant.

2. Aslamazov-Larkin diagrams

In this section, we evaluate the contribution of AL diagrams in [Figs. 6(e) and 6(f)]. The sum of the two diagrams can be written as

$$\delta\chi_c^{\rm AL}(\mathbf{q},\omega_m) = (N_sN_v)^2\int\frac{d^2Q}{(2\pi)^2}\int\frac{d\Omega_l}{2\pi}[\mathcal{T}^2(\mathbf{Q},\mathbf{q},\Omega_l,\omega_m)+|\mathcal{T}(\mathbf{Q},\mathbf{q},\Omega_l,\omega_m)|^2]U(\mathbf{Q},\Omega_l)U(\mathbf{Q}-\mathbf{q},\Omega_l-\omega_m), \tag{D10}$$

where N_s and N_v are the spin and valley degeneracies, respectively, and

$$\mathcal{T}(\mathbf{Q},\mathbf{q},\Omega_l,\omega_m) = \int\frac{d^2k}{(2\pi)^2}\frac{d\varepsilon_n}{2\pi}G(\mathbf{k},\varepsilon_n)G(\mathbf{k}+\mathbf{q},\varepsilon_n+\omega_m)G(\mathbf{k}+\mathbf{Q},\varepsilon_n+\Omega_l) \tag{D11}$$

is the "triangular" part of the diagram. The combination $\mathcal{T}^2+|\mathcal{T}|^2$ can be rewritten identically as $2\,\mathrm{Re}\mathcal{T}^2+2i\,\mathrm{Re}\mathcal{T}\,\mathrm{Im}\mathcal{T}$. Because any physical susceptibility is purely real on the Matsubara axis, the imaginary part of $\mathcal{T}^2+|\mathcal{T}|^2$ must vanish upon integrations, and thus can be omitted. Therefore, we need to find only $\mathrm{Re}\mathcal{T}$.

Integrating over ε_n, we obtain

$$\mathcal{T}(\mathbf{Q},\mathbf{q},\Omega_l,\omega_m) = \int\frac{d^2k}{(2\pi)^2}\frac{1}{i\omega_m-\epsilon_{\mathbf{k}+\mathbf{q}}+\epsilon_{\mathbf{k}}}\left[\frac{n_{\mathbf{k}}-n_{\mathbf{k}+\mathbf{Q}}}{i\Omega_l-\epsilon_{\mathbf{k}+\mathbf{Q}}+\epsilon_{\mathbf{k}}}-\frac{n_{\mathbf{k}+\mathbf{q}}-n_{\mathbf{k}+\mathbf{Q}}}{i(\Omega_l-\omega_m)-\epsilon_{\mathbf{k}+\mathbf{Q}}+\epsilon_{\mathbf{k}+\mathbf{q}}}\right]. \tag{D12}$$

From this point on, the calculation proceeds along a different route compared to the one for the self-energy and exchange diagrams. Namely, if the single-particle dispersion is expanded to linear order in q and Q, we will get a zero result for $\mathrm{Re}\mathcal{T}$. This is a reflection of a known fact that AL diagrams hinge on violating particle-hole symmetry [82]. To get a nonzero result, we need to keep $O(Q^2)$ terms in the dispersion. However, we can ignore $O(q^2)$ terms because q can be chosen arbitrarily small. For doped graphene, such an expansion amounts to $\epsilon_{\mathbf{k}+\mathbf{Q}}\approx\epsilon_{\mathbf{k}}+\mathbf{v}_{\mathbf{k}}\cdot\mathbf{Q}+Q^2\sin^2\theta/2m^*$, where $m^*=k_{\rm F}/v_{\rm D}$ and θ is the angle between $\mathbf{Q}$ and $\mathbf{k}$.

Expanding the Fermi functions in Eq. (D12) to order Q^2, we obtain

$$\mathcal{T}(\mathbf{Q},\mathbf{q},\Omega_l,\omega_m) = \int\frac{d^2k}{(2\pi)^2}\frac{1}{i\omega_m-\mathbf{v}_{\mathbf{k}}\cdot\mathbf{q}}\left[\frac{\left(\mathbf{v}_{\mathbf{k}}\cdot\mathbf{Q}+\frac{Q^2}{2m^*}\sin^2\theta\right)(-n'_{\mathbf{k}})-\frac{1}{2}(\mathbf{v}_{\mathbf{k}}\cdot\mathbf{Q})^2n''_{\mathbf{k}}}{i\Omega_l-\mathbf{v}_{\mathbf{k}}\cdot\mathbf{Q}-\frac{Q^2}{2m^*}\sin^2\theta} - \frac{\left[\mathbf{v}_{\mathbf{k}}\cdot(\mathbf{q}-\mathbf{Q})+\frac{Q^2}{2m^*}\sin^2\theta\right]n'_{\mathbf{k}}-\frac{1}{2}(\mathbf{v}_{\mathbf{k}}\cdot\mathbf{Q})^2n''_{\mathbf{k}}}{i(\Omega_l-\omega_m)-\mathbf{v}_{\mathbf{k}}\cdot(\mathbf{q}-\mathbf{Q})-\frac{Q^2}{2m^*}\sin^2\theta}\right]. \tag{D13}$$

It is convenient to separate $\mathcal{T}$ into two parts as $\mathcal{T}=\mathcal{T}_1+\mathcal{T}_2$, where $\mathcal{T}_1$ and $\mathcal{T}_2$ contain terms proportional to $n'_{\mathbf{k}}$ and $n''_{\mathbf{k}}$, respectively. At $T=0$, $n'_{\mathbf{k}}=-\delta(\epsilon_{\mathbf{k}}-\mu)$ and $n''_{\mathbf{k}}=-\delta'(\epsilon_{\mathbf{k}}-\mu)$, so that

$$\mathcal{T}_1(\mathbf{Q},\mathbf{q},\Omega_l,\omega_m) = \int\frac{d^2k}{(2\pi)^2}\frac{\delta(\epsilon_{\mathbf{k}}-\mu)}{i\omega_m-\mathbf{v}_{\mathbf{k}}\cdot\mathbf{q}}\left[\frac{\mathbf{v}_{\mathbf{k}}\cdot\mathbf{Q}+\frac{Q^2}{2m^*}\sin^2\theta}{i\Omega_l-\mathbf{v}_{\mathbf{k}}\cdot\mathbf{Q}-\frac{Q^2}{2m^*}\sin^2\theta}+\frac{\mathbf{v}_{\mathbf{k}}\cdot(\mathbf{q}-\mathbf{Q})+\frac{Q^2}{2m^*}\sin^2\theta}{i(\Omega_l-\omega_m)-\mathbf{v}_{\mathbf{k}}\cdot(\mathbf{q}-\mathbf{Q})-\frac{Q^2}{2m^*}\sin^2\theta}\right],$$

$$\mathcal{T}_2(\mathbf{Q},\mathbf{q},\Omega_l,\omega_m) = \frac{1}{2}\int\frac{d^2k}{(2\pi)^2}\frac{\delta'(\epsilon_{\mathbf{k}}-\mu)(\mathbf{v}_{\mathbf{k}}\cdot\mathbf{Q})^2}{i\omega_m-\mathbf{v}_{\mathbf{k}}\cdot\mathbf{q}}\left[\frac{1}{i\Omega_l-\mathbf{v}_{\mathbf{k}}\cdot\mathbf{Q}}-\frac{1}{i(\Omega_l-\omega_m)-\mathbf{v}_{\mathbf{k}}\cdot\mathbf{Q}+\mathbf{v}_{\mathbf{k}}\cdot\mathbf{q}}\right]. \tag{D14}$$

We neglected the $O(Q^2)$ terms in the denominators of both two parts of $\mathcal{T}_2$ because $\mathcal{T}_2$ is already proportional to Q^2. Now we integrate over $\epsilon_{\mathbf{k}}$ in Eq. (D14) to obtain

$$\mathcal{T}_1(\mathbf{Q},\mathbf{q},\Omega_l,\omega_m) = N_\mathrm{F}\int\frac{d\theta}{2\pi}\frac{1}{i\omega_m - v_\mathrm{D}\hat{\mathbf{k}}\cdot\mathbf{q}}\left[\frac{v_\mathrm{D}\hat{\mathbf{k}}\cdot\mathbf{Q}+\frac{Q^2}{2m^*}\sin^2\theta}{i\Omega_l - v_\mathrm{D}\hat{\mathbf{k}}\cdot\mathbf{Q}-\frac{Q^2}{2m^*}\sin^2\theta}+\frac{v_\mathrm{D}\hat{\mathbf{k}}\cdot(\mathbf{q}-\mathbf{Q})+\frac{Q^2}{2m^*}\sin^2\theta}{i(\Omega_l-\omega_m)-v_\mathrm{D}\hat{\mathbf{k}}\cdot(\mathbf{q}-\mathbf{Q})-\frac{Q^2}{2m^*}\sin^2\theta}\right],$$

$$\mathcal{T}_2(\mathbf{Q},\mathbf{q},\Omega_l,\omega_m) = -\frac{1}{4\pi}\int\frac{d\theta}{2\pi}\frac{(\hat{\mathbf{k}}\cdot\mathbf{Q})^2}{i\omega_m - v_\mathrm{D}\hat{\mathbf{k}}\cdot\mathbf{q}}\left[\frac{1}{i\Omega_l - v_\mathrm{D}\hat{\mathbf{k}}\cdot\mathbf{Q}}-\frac{1}{i(\Omega_l-\omega_m)-v_\mathrm{D}\hat{\mathbf{k}}\cdot\mathbf{Q}+v_\mathrm{D}\hat{\mathbf{k}}\cdot\mathbf{q}}\right]. \quad \text{(D15)}$$

Since we are interested in the regime of $qv_\mathrm{D}\ll\omega$, the equations above can be expanded in q. While doing so, we will be discarding imaginary parts of $\mathcal{T}_{1,2}$ because they must vanish on subsequent integrations anyway. The leading-order results of such an expansion read as

$$\begin{aligned}\mathrm{Re}\mathcal{T}_1(\mathbf{Q},\mathbf{q},\Omega_l,\omega_m) &= N_\mathrm{F}\frac{Q^2}{2m^*}\int\frac{d\theta}{2\pi}(v_\mathrm{D}\hat{\mathbf{k}}\cdot\mathbf{q})\sin^2\theta\\ &\quad\times\left[\frac{1}{(i\omega_m)^2}\left(\frac{1}{i\Omega_l - v_\mathrm{D}\hat{\mathbf{k}}\cdot\mathbf{Q}}-\frac{1}{i(\Omega_l-\omega_m)-v_\mathrm{D}\hat{\mathbf{k}}\cdot\mathbf{Q}}+\frac{v_\mathrm{D}\hat{\mathbf{k}}\cdot\mathbf{Q}}{(i\Omega_l-v_\mathrm{D}\hat{\mathbf{k}}\cdot\mathbf{Q})^2}-\frac{v_\mathrm{D}\hat{\mathbf{k}}\cdot\mathbf{Q}}{[i(\Omega_l-\omega_m)-v_\mathrm{D}\hat{\mathbf{k}}\cdot\mathbf{Q}]^2}\right)\right.\\ &\quad\left.+\frac{2}{i\omega_m}\left(\frac{1}{(i(\Omega_l-\omega_m)-v_\mathrm{D}\hat{\mathbf{k}}\cdot\mathbf{Q})^2}+\frac{v_\mathrm{D}\hat{\mathbf{k}}\cdot\mathbf{Q}}{[i(\Omega_l-\omega_m)-v_\mathrm{D}\hat{\mathbf{k}}\cdot\mathbf{Q}]^3}\right)\right],\\ \mathrm{Re}\mathcal{T}_2(\mathbf{Q},\mathbf{q},\Omega_l,\omega_m) &= -\frac{1}{4\pi}\int\frac{d\theta}{2\pi}(\hat{\mathbf{k}}\cdot\mathbf{q})(\hat{\mathbf{k}}\cdot\mathbf{Q})^2\\ &\quad\times\left[\frac{1}{(i\omega_m)^2}\left(\frac{1}{i\Omega_l - v_\mathrm{D}\hat{\mathbf{k}}\cdot\mathbf{Q}}-\frac{1}{i(\Omega_l-\omega_m)-v_\mathrm{D}\hat{\mathbf{k}}\cdot\mathbf{Q}}\right)+\frac{1}{i\omega_m}\left(\frac{1}{[i(\Omega_l-\omega_m)-v_\mathrm{D}\hat{\mathbf{k}}\cdot\mathbf{Q}]^2}\right)\right],\end{aligned} \quad \text{(D16)}$$

where $N_\mathrm{F}=m^*/4\pi$ is the density of states per spin and per valley. Now we integrate over θ (the angle between $\mathbf{k}$ and $\mathbf{Q}$) to obtain

$$\mathrm{Re}\mathcal{T}(\mathbf{Q},\mathbf{q},\Omega_l,\omega_m) = \frac{\mathbf{q}\cdot\mathbf{Q}}{4\pi\omega_m^2(v_\mathrm{D}Q)^2}\left(|\Omega_l|\sqrt{\Omega_l^2+(v_\mathrm{D}Q)^2}-|\Omega_l-\omega_m|\sqrt{(\Omega_l-\omega_m)^2+(v_\mathrm{D}Q)^2}+(\Omega_l-\omega_m)^2-\Omega_l^2\right). \quad \text{(D17)}$$

Substituting the last result back into Eq. (D10) and rescaling the variables as $x=\Omega_l/v_\mathrm{D}Q$ and $y=\omega_m/v_\mathrm{D}Q$, we find

$$\begin{aligned}\chi_c^\mathrm{AL}(\mathbf{q},\omega_m) &= \frac{2(N_sN_v)^2}{16\pi^2\omega_m^4}\int\frac{d^2Q}{(2\pi)^2}\int\frac{dx}{2\pi}\frac{2\pi e^2}{Q+\kappa\left(1-\frac{|x|}{\sqrt{x^2+1}}\right)}\frac{2\pi e^2}{Q+\kappa\left(1-\frac{|x-y|}{\sqrt{(x-y)^2+1}}\right)}\\ &\quad\times(\mathbf{q}\cdot\mathbf{Q})^2v_\mathrm{D}Q\left(|x|\sqrt{x^2+1}-|x-y|\sqrt{(x-y)^2+1}+(x-y)^2-x^2\right)^2.\end{aligned} \quad \text{(D18)}$$

Now we will simplify the last equation assuming that $\Omega_l\sim\omega_m\ll v_\mathrm{D}Q$. Our goal is to find the imaginary part of χ_c^irr after analytic continuation, while Eq. (D18) is proportional to the even (fourth) power of ω_m, which remains real after analytic continuation. Therefore, when expanding the integrand of Eq. (D18) in $\Omega_l/v_\mathrm{D}Q$ and $\omega_m/v_\mathrm{D}Q$, we need to keep those terms that will be integrated into odd powers of ω_m. To order ω_m^5, the integral over x is solved as

$$\begin{aligned}I_\mathrm{AL} &= \int_{-\infty}^{\infty}dx\left(\frac{1}{(Q+\kappa)^2}+\frac{\kappa}{(Q+\kappa)^3}(|x|+|x+y|)+\frac{\kappa^2}{(Q+\kappa)^4}[x^2+(x-y)^2+|x||x-y|]\right)\\ &\quad\times\left[|x|\left(1+\frac{x^2}{2}\right)-|x-y|\left(1+\frac{(x-y)^2}{2}\right)-2xy+y^2\right]^2\\ &= O(y^2)-\frac{2}{3(Q+\kappa)^2}y^3+O(y^4)-\frac{2\kappa^2}{5(Q+\kappa)^4}y^5,\end{aligned} \quad \text{(D19)}$$

where we spelled out only the odd in ω_m terms. Substituting the y^3 and y^5 terms into Eq. (D18), we get

$$\chi_c^\mathrm{AL}(\mathbf{q},\omega_m) = -\frac{e^4}{\pi^2v_\mathrm{D}^2}\left[\frac{2}{3}\frac{q^2}{\omega_m}\int_0^{\Lambda_Q}\frac{dQ\,Q}{(Q+\kappa)^2}+\frac{2}{5}\frac{q^2\omega_m\kappa^2}{v_\mathrm{D}^2}\int_{|\omega_m|/v_\mathrm{D}}^{\infty}\frac{dQ}{Q}\frac{1}{(Q+\kappa)^4}\right], \quad \text{(D20)}$$

where we used that $N_s=N_v=2$ for graphene.

Now see that the first terms in Eq. (D9) for the self-energy and exchange diagrams and Eq. (D20) cancel each other. Solving the remaining integral over Q to leading-logarithm order and using $\kappa=4m^*e^2$, we obtain the final result:

$$\chi_c^\mathrm{irr}(\mathbf{q},\omega_m) = -\frac{q^2\omega_m}{80\pi^2\mu^2}\ln\frac{v_\mathrm{D}\kappa}{|\omega_m|}. \quad \text{(D21)}$$

Carrying out analytical continuation and taking the imaginary part of the result, we arrive at Eq. (84) of the main text.

APPENDIX E: OPTICAL CONDUCTIVITY OF BILAYER GRAPHENE

We use the model of BLG, which includes intralayer hopping between A and B sites (with coupling γ_0), interlayer hopping between the nearest A sites and the nearest B sites (with couplings γ_1 and γ_3, respectively), but neglects interlayer hopping between A and B sites [60]. In this model, the lowest branch of the conduction band is given by

$$\epsilon^{+}_{\varsigma,\mathbf{k}} = \left\{\frac{\gamma_1^2}{2} + \left(v_D^2 - \frac{v_3^2}{2}\right)k^2 - \left[\frac{\gamma_1^4}{4} + \gamma_1^2\left(v_D^2 - \frac{v_3^2}{2}\right)k^2 + 2\varsigma v_3 v_D^2 k^3\cos 3\theta_{\mathbf{k}} + v_3^2\left(v_D^2 + \frac{v_3^2}{4}\right)k^4\right]^{1/2}\right\}^{1/2}, \quad \text{(E1)}$$

where, as before, $v_D = 3\gamma_0 a/2$ and $v_3 = 3\gamma_3 a/2$. For a realistic BLG, $\gamma_1 \sim \gamma_3 \ll \gamma_0$ (Ref. [60]) and, therefore, $v_3 \ll v_D$. For $\gamma_1 \ll \mu \ll \gamma_0$ the states near the FS have a Dirac dispersion with a slope of v_D, and we are back to the case of monolayer graphene (MLG), discussed in Sec. III B. For $\mu \ll \gamma_1$, all the k-dependent terms under $[\dots]^{1/2}$ in Eq. (E1) are subleading to the γ_1^4 term. Expanding $[\dots]^{1/2}$ to order k^6 and neglecting v_3 compared to v_D whenever possible, we obtain

$$\epsilon^{+}_{\varsigma,\mathbf{k}} = \left\{v_3^2k^2 + \left(\frac{k^2}{2\tilde{m}}\right)^2 - \frac{2\varsigma v_D^2 v_3 k^3}{\gamma_1}\cos 3\theta_{\mathbf{k}} - \frac{2v_D^6k^6}{\gamma_1^4}\right\}^{1/2}, \quad \text{(E2)}$$

where $\varsigma = \pm 1$ denotes the $K_\pm$ point. For $\mu \ll \tilde{m}v_3^2$ the first term under the square root in the equation above is the dominant one, and we are again back to a Dirac dispersion, but with a slope of v_3 rather than v_D. This is another case of a DFL discussed in Sec. III B. A specific to BLG regime occurs for $\tilde{m}v_3^2 \ll \mu \ll \gamma_1$. In this regime the quartic term is the dominant one. Expanding to first order in the subleading terms and omitting a constant, $\tilde{m}v_3^2$ term, we obtain

$$\epsilon_{\varsigma\mathbf{k}} = \frac{k^2}{2\tilde{m}} - \varsigma v_3 k\cos 3\theta_{\mathbf{k}} - \frac{k^4}{4\tilde{m}^2\gamma_1}. \quad \text{(E3)}$$

The first term in the equation above corresponds to a Galilean-invariant FL with $\mathrm{Re}\sigma(\omega, T) = 0$. The second, anisotropic term gives rise to a finite $\mathrm{Re}\sigma(\omega, T)$, described by the Gurzhi formula (1), as in the case of MLG with trigonal warping, discussed in Sec. III C, the mechanism of dissipation is *ee* scattering between nondegenerate valleys. For $\mu \gg \tilde{m}v_3^2$, the second term is smaller than the first one. Finally, the last term is an isotropic correction to the quadratic dispersion, which gives rise to a finite $\mathrm{Re}\sigma(\omega, T)$, described by the DFL form (45). Therefore, the conductivity of BLG has the same general form as in Eqs. (51) and (52) for MLG, but with different coefficients. To estimate the coefficient of the DFL part, we neglect the trigonal-warping term in Eq. (E3) and treat the quartic term as a correction to the quadratic one. Equation (39) then gives the nonparabolicity coefficient as $|w| = 4\mu/\gamma_1 \ll 1$. On the other hand, the coefficient of the Gurzhi part is proportional to the magnitude of the trigonal-warping term in Eq. (E3), i.e., to $(v_3/v_D)^2$, where $v_F = k_D/\tilde{m}$. Combining the two contributions, we obtain the result in Eq. (96) of the main text.

[1] R. Gurzhi, Zh. Eksp. Teor. Fiz. **35**, 965 (1959) [JETP **35**, 673 (1959)].
[2] H. Pal, V. Yudson, and D. Maslov, Lith. J. Phys. **52**, 142 (2012).
[3] D. L. Maslov and A. V. Chubukov, Rep. Prog. Phys. **80**, 026503 (2016).
[4] R. Gurzhi, A. Kopeliovich, and S. Rutkevich, ZhETF **83**, 290 (1982) [JETP Lett. **56**, 159 (1982)].
[5] R. N. Gurzhi, A. Kopeliovich, and S. B. Rutkevich, Adv. Phys. **36**, 221 (1987).
[6] R. N. Gurzhi, A. N. Kalinenko, and A. I. Kopeliovich, Phys. Rev. B **52**, 4744 (1995).
[7] A. Rosch and P. C. Howell, Phys. Rev. B **72**, 104510 (2005).
[8] A. Rosch, Ann. Phys. **15**, 526 (2006).
[9] D. L. Maslov, V. I. Yudson, and A. V. Chubukov, Phys. Rev. Lett. **106**, 106403 (2011).
[10] U. Briskot, M. Schütt, I. V. Gornyi, M. Titov, B. N. Narozhny, and A. D. Mirlin, Phys. Rev. B **92**, 115426 (2015).
[11] P. J. Ledwith, H. Guo, and L. Levitov, Ann. Phys. **411**, 167913 (2019).
[12] A. V. Chubukov and D. L. Maslov, Phys. Rev. B **86**, 155136 (2012); D. L. Maslov and A. V. Chubukov, *ibid.* **86**, 155137 (2012).
[13] A. H. Castro Neto, F. Guinea, N. M. R. Peres, K. S. Novoselov, and A. K. Geim, Rev. Mod. Phys. **81**, 109 (2009).
[14] M. Z. Hasan and C. L. Kane, Rev. Mod. Phys. **82**, 3045 (2010).
[15] O. Vafek and A. Vishwanath, Annu. Rev. Condens. Matter Phys. **5**, 83 (2014).
[16] A. Burkov, Annu. Rev. Condens. Matter Phys. **9**, 359 (2018).
[17] N. P. Armitage, E. J. Mele, and A. Vishwanath, Rev. Mod. Phys. **90**, 015001 (2018).
[18] N. M. R. Peres, Rev. Mod. Phys. **82**, 2673 (2010).
[19] S. Das Sarma, S. Adam, E. H. Hwang, and E. Rossi, Rev. Mod. Phys. **83**, 407 (2011).
[20] V. N. Kotov, B. Uchoa, V. M. Pereira, F. Guinea, and A. H. Castro Neto, Rev. Mod. Phys. **84**, 1067 (2012).
[21] K. F. Mak, L. Ju, F. Wang, and T. F. Heinz, Solid State Commun. **152**, 1341 (2012).
[22] A. W. W. Ludwig, M. P. A. Fisher, R. Shankar, and G. Grinstein, Phys. Rev. B **50**, 7526 (1994).
[23] T. Ando, Y. Zheng, and H. Suzuura, J. Phys. Soc. Jpn. **71**, 1318 (2002).
[24] V. P. Gusynin, S. G. Sharapov, and J. P. Carbotte, Phys. Rev. Lett. **96**, 256802 (2006).

[25] L. A. Falkovsky and A. A. Varlamov, Eur. Phys. J. B **56**, 281 (2007).
[26] K. S. Novoselov, A. K. Geim, S. V. Morozov, D. Jiang, Y. Zhang, S. V. Dubonos, I. V. Grigorieva, and A. A. Firsov, Science **306**, 666 (2004).
[27] Z. Q. Li, E. A. Henriksen, Z. Jiang, Z. Hao, M. C. Martin, P. Kim, H. L. Stormer, and D. N. Basov, Nat. Phys. **4**, 532 (2008).
[28] K. F. Mak, M. Y. Sfeir, Y. Wu, C. H. Lui, J. A. Misewich, and T. F. Heinz, Phys. Rev. Lett. **101**, 196405 (2008).
[29] R. R. Nair, P. Blake, A. N. Grigorenko, K. S. Novoselov, T. J. Booth, T. Stauber, N. M. R. Peres, and A. K. Geim, Science **320**, 1308 (2008).
[30] J. Horng, C.-F. Chen, B. Geng, C. Girit, Y. Zhang, Z. Hao, H. A. Bechtel, M. Martin, A. Zettl, M. F. Crommie, Y. R. Shen, and F. Wang, Phys. Rev. B **83**, 165113 (2011).
[31] E. G. Mishchenko, Phys. Rev. Lett. **98**, 216801 (2007).
[32] D. E. Sheehy and J. Schmalian, Phys. Rev. Lett. **99**, 226803 (2007).
[33] E. G. Mishchenko, Europhys. Lett. **83**, 17005 (2008).
[34] A. B. Kashuba, Phys. Rev. B **78**, 085415 (2008).
[35] L. Fritz, J. Schmalian, M. Müller, and S. Sachdev, Phys. Rev. B **78**, 085416 (2008).
[36] I. F. Herbut, V. Juričić, and O. Vafek, Phys. Rev. Lett. **100**, 046403 (2008).
[37] S. H. Abedinpour, G. Vignale, A. Principi, M. Polini, W.-K. Tse, and A. H. MacDonald, Phys. Rev. B **84**, 045429 (2011).
[38] I. Sodemann and M. M. Fogler, Phys. Rev. B **86**, 115408 (2012).
[39] N. M. R. Peres, J. M. B. Lopes dos Santos, and T. Stauber, Phys. Rev. B **76**, 073412 (2007).
[40] T. Stauber, N. M. R. Peres, and A. H. Castro Neto, Phys. Rev. B **78**, 085418 (2008).
[41] N. M. R. Peres, T. Stauber, and A. H. C. Neto, Europhys. Lett. **84**, 38002 (2008).
[42] N. M. R. Peres, R. M. Ribeiro, and A. H. Castro Neto, Phys. Rev. Lett. **105**, 055501 (2010).
[43] A. G. Grushin, B. Valenzuela, and M. A. H. Vozmediano, Phys. Rev. B **80**, 155417 (2009).
[44] A. Principi, G. Vignale, M. Carrega, and M. Polini, Phys. Rev. B **88**, 195405 (2013).
[45] W. Götze and P. Wölfle, Phys. Rev. B **6**, 1226 (1972).
[46] M. Müller, L. Fritz, and S. Sachdev, Phys. Rev. B **78**, 115406 (2008).
[47] S. A. Jafari and G. Baskaran, J. Phys.: Condens. Matter **24**, 095601 (2012).
[48] A. A. Abrikosov, Zh. Eksp. Teor. Fiz. **44**, 2039 (1963) [JETP **17**, 1372 (1963)].
[49] E. G. Mishchenko, M. Y. Reizer, and L. I. Glazman, Phys. Rev. B **69**, 195302 (2004).
[50] A. V. Chaplik, Zh. Eksp. Teor. Fiz. **60**, 1845 (1971) [JETP **33**, 997 (1971)].
[51] G. F. Giuliani and J. J. Quinn, Phys. Rev. B **26**, 4421 (1982).
[52] E. M. Lifshitz and L. P. Pitaevskii, *Physical Kinetics, Course of Theoretical Physics, Volume X* (Butterworth-Heinemann, Burlington, 1981).
[53] J. Rammer and H. Smith, Rev. Mod. Phys. **58**, 323 (1986).
[54] R. N. Gurzhi, Phys. Usp. **11**, 255 (1968).
[55] M. Mitrano, A. A. Husain, S. Vig, A. Kogar, M. S. Rak, S. I. Rubeck, J. Schmalian, B. Uchoa, J. Schneeloch, R. Zhong, G. D. Gu, and P. Abbamonte, Proc. Natl. Acad. Sci. USA **115**, 5392 (2018).
[56] A. A. Husain, M. Mitrano, M. S. Rak, S. I. Rubeck, H. Yang, C. Sow, Y. Maeno, P. E. Batson, and P. Abbamonte, arXiv:2007.06670.
[57] E. W. Huang, K. Limtragool, C. Setty, A. A. Husain, M. Mitrano, P. Abbamonte, and P. W. Phillips, Phys. Rev. B **103**, 035121 (2021).
[58] V. A. Zyuzin, P. Sharma, and D. L. Maslov, Phys. Rev. B **98**, 115139 (2018).
[59] P. Sharma, A. Principi, G. Vignale, and D. L. Maslov (unpublished).
[60] E. McCann and M. Koshino, Rep. Prog. Phys. **76**, 056503 (2013).
[61] L. Fu, Phys. Rev. Lett. **103**, 266801 (2009).
[62] H. K. Pal, V. I. Yudson, and D. L. Maslov, Phys. Rev. B **85**, 085439 (2012).
[63] P. Hosur and X. Qi, C. R. Phys. **14**, 857 (2013).
[64] P. E. C. Ashby and J. P. Carbotte, Phys. Rev. B **89**, 245121 (2014).
[65] M. Orlita, D. M. Basko, M. S. Zholudev, F. Teppe, W. Knap, V. I. Gavrilenko, N. N. Mikhailov, S. A. Dvoretskii, P. Neugebauer, C. Faugeras, A.-L. Barra, G. Martinez, and M. Potemski, Nat. Phys. **10**, 233 (2014).
[66] R. Y. Chen, S. J. Zhang, J. A. Schneeloch, C. Zhang, Q. Li, G. D. Gu, and N. L. Wang, Phys. Rev. B **92**, 075107 (2015).
[67] A. B. Sushkov, J. B. Hofmann, G. S. Jenkins, J. Ishikawa, S. Nakatsuji, S. Das Sarma, and H. D. Drew, Phys. Rev. B **92**, 241108(R) (2015).
[68] G. S. Jenkins, C. Lane, B. Barbiellini, A. B. Sushkov, R. L. Carey, F. Liu, J. W. Krizan, S. K. Kushwaha, Q. Gibson, T.-R. Chang, H.-T. Jeng, H. Lin, R. J. Cava, A. Bansil, and H. D. Drew, Phys. Rev. B **94**, 085121 (2016).
[69] D. Neubauer, J. P. Carbotte, A. A. Nateprov, A. Löhle, M. Dressel, and A. V. Pronin, Phys. Rev. B **93**, 121202(R) (2016).
[70] D. K. Efetov and P. Kim, Phys. Rev. Lett. **105**, 256805 (2010).
[71] D. R. Cooper, B. D'Anjou, N. Ghattamaneni, B. Harack, M. Hilke, A. Horth, N. Majlis, M. Massicotte, L. Vandsburger, E. Whiteway, and V. Yu, ISRN Condens. Matter Phys. **2012**, 501686 (2012).
[72] I. Childres, L. A. Jauregui, W. Park, H. Cao, and Y. P. Chen, *New Developments in Photon and Materials Research*, Vol. 1 (Nova Science, Hauppauge, NY, 2013).
[73] R. T. Beach and R. W. Christy, Phys. Rev. B **16**, 5277 (1977).
[74] G. R. Parkins, W. E. Lawrence, and R. W. Christy, Phys. Rev. B **23**, 6408 (1981).
[75] E. H. Hwang and S. Das Sarma, Phys. Rev. B **77**, 115449 (2008).
[76] S. V. Morozov, K. S. Novoselov, M. I. Katsnelson, F. Schedin, D. C. Elias, J. A. Jaszczak, and A. K. Geim, Phys. Rev. Lett. **100**, 016602 (2008).
[77] J.-H. Chen, C. Jang, S. Xiao, M. Ishigami, and M. S. Fuhrer, Nat. Nanotechnol. **3**, 206 (2008).
[78] E. V. Castro, H. Ochoa, M. I. Katsnelson, R. V. Gorbachev, D. C. Elias, K. S. Novoselov, A. K. Geim, and F. Guinea, Phys. Rev. Lett. **105**, 266601 (2010).
[79] S. Fratini and F. Guinea, Phys. Rev. B **77**, 195415 (2008).
[80] E. H. Hwang and S. Das Sarma, Phys. Rev. B **79**, 165404 (2009).
[81] G. D. Mahan, *Many-Particle Physics*, 3rd ed. (Kluwer, Dordrecht, 2000).
[82] A. Kamenev and Y. Oreg, Phys. Rev. B **52**, 7516 (1995).